2015

The effect of sequence and environment on the structure and dimerization of amyloid precursor protein

BOSTON UNIVERSITY

GRADUATE SCHOOL OF ARTS AND SCIENCES

Dissertation

THE EFFECT OF SEQUENCE AND ENVIRONMENT ON THE STRUCTURE AND DIMERIZATION OF AMYLOID PRECURSOR PROTEIN

by

LEIGH S. HOLMES FOSTER

B.A., Mount Holyoke College, 2008
M.A., Boston University, 2010

Submitted in partial fulfillment of the

requirements for the degree of

Doctor of Philosophy

2015

Approved by

First Reader _____

John E. Straub, Ph.D.
Professor of Chemistry

Second Reader _____

Sandor Vajda, Ph.D.
Professor of Chemistry

Third Reader _____

Adrian Whitty, Ph.D.
Professor of Chemistry

Acknowledgements

But I make a profit of three and a quarter cents an egg by selling them for four and a quarter cents an egg to the people in Malta I buy them from for seven cents an egg. Of course, I don't make the profit. The syndicate makes the profit. And everybody has a share.

Joseph Heller

There are many people who deserve a share in my graduate school experience. First, thank you to my advisor, John Straub, for welcoming me to the lab, and for all your help throughout my time there. Thank you to Adrian Whitty for the many pep talks and words of wisdom and support over the years. And to all my committee members: Sandor Vajda, Karen Allen, and David Coker, thank you all for your support and guidance through this process.

There have been so many people in the Straub Lab who have helped me get to where I am today. Edyta Małolepza and Laura Domínguez, I honestly don't know what I would have done without the two of you. Thank you to Anna Victoria Martinez, Qing Lu, Lani Rush, Adam Moser, and everyone who has been in the lab for all the long lunches and ridiculous conversations over the years.

There almost isn't enough space to thank all the people graduate school brought into my life. Katie Summo, you've kept me sane, I'm glad you lost that pool game. Natalya Bassina and all the CH101/102 TFs and LAs, thank you for the joy of working with all of you. And thank you to all my fellow grad students who have laughed and commiserated with me and made this whole endeavor bearable.

Thank you to my parents, and to my family and friends who have all been there for me and believed in me every step of the way. Finally, I would like to thank my wonderful wife Kelsey, who has been the most constant source of love and support through this entire experience. I couldn't have done it without you.

THE EFFECT OF SEQUENCE AND ENVIRONMENT ON THE STRUCTURE AND DIMERIZATION OF AMYLOID PRECURSOR PROTEIN

(Order No.)

LEIGH S. HOLMES FOSTER

Boston University Graduate School of Arts and Sciences, 2015

Major Professor: John E. Straub, Professor of Chemistry

ABSTRACT

Aggregation of amyloid β (Aβ) protein has been linked to the development of Alzheimer's Disease (AD). The genesis of Aβ involves the cleavage Amyloid Precursor Protein (APP) by β-secretase, producing the 99-residue C99 peptide, and the subsequent cleavage of C99 by γ-secretase to produce Aβ. A detailed understanding of the γ-cleavage process is essential to our undertsanding of the pathological mechanisms linking the aggregation of Aβ to the development of AD. This work seeks to provide insight into critical aspects of the structure and dynamics of C99, and the particular roles played by (1) C99 amino acid sequence and (2) the lipid composition of the membrane environment. Many studies have focused on the importance of the C99 sequence, including known studies of Familial AD (FAD) mutants as well as engineered mutations. Specific mutations have been found to affect the processing of C99, which has been linked to changes in the structure of C99 and the formation of C99 homodimers. Similarly, changes in the membrane environment, through variation in lipid composition and the presence of cholesterol, have been found to affect C99 structure and positioning within the membrane as well as C99 dimerization.

The results of this work extend our understanding of the APP-C99 system and its interaction with the environment. Using a multiscale simulation approach, we find key structural effects of engineered mutations that suggest possible mechanistic insight into the γ-cleavage process. Using C99 congener peptides, we examine the effect of local membrane environment on the dimerization of C99, focusing on the roles of both the transmembrane

(TM) region as well as the juxtamembrane (JM) domain. Further studies characterize the role of a FAD mutation, and demonstrate the effect of the mutation on the dimerization of C99 in agreement with experimental findings. Overall, this work leads to critical insight into the role of sequence and membrane on the structure of C99 in a membrane environment, and provides support for the conjecture that the structure of C99 monomer and homodimer are critical to our understanding of the processing of C99, a critical step in the genesis of Aβ peptide and the etiology of Alzheimer's Disease.

Contents

List of Tables

List of Figures

List of Abbreviations

Aβ	.....	amyloid-β
AD	.....	Alzheimer's Disease
AICD	.....	Amyloid intracellular domain
APP	.....	Amyloid Precursor Protein
CHC	.....	central hydrophobic core
C99	.....	APP-C99 peptide
DHPC	.....	1,2-diheptanoyl-sn-glycero-3-phosphocholine
DMPC	.....	1,2-dimyristoyl-sn-glycero-3-phosphocholine
DMPG	.....	1,2-dimyristoyl-sn-glycero-3-phospho-(1'-rac-glycerol)
DOPE	.....	1,2-dioleoyl-sn-glycero-3-phosphoethanolamine
DPC	.....	n-dodecylphosphocholine
DPPC	.....	1,2-dipalmitoyl-sn-glycero-3-phosphocholine
EphA2	.....	Ephrin type-A receptor 2
FAD	.....	Familial Alzheimer's Disease
GpA	.....	Glycophorin A
LMPG	.....	lysomyristoylphosphatidylglycerol
MD	.....	molecular dynamics
POPC	.....	1-palmitoyl-2-oleoyl-sn-glycero-3-phosphocholine
PS1	.....	Presenilin 1
TM	.....	transmembrane
WT	.....	wild type

Chapter 1

Alzheimer's Disease and Aβ

Senile dementia is by no means a new condition. The progression of dementia with increasing age has been noted since antiquity; a problem whose severity has only increased along with average life expectancies. In 1906, Aloys Alzheimer was the first to characterize a pathological marker associated with dementia [1, 2]. While examining the brain of a woman who had died after years of dementia, he found neural plaques and fibrils; factors which would become the hallmark of Alzheimer's Disease (AD) - named for his discovery. Continuing research into these markers picked up in the 1960s, when Terry and Kidd published electron microscopy studies of AD cytopathology [3, 4]. These studies provided the background for the 1984 work by Glenner and Wong at UCSD which uncovered the amyloid core of these fibrils [5]. This discovery paved the road for the identification of the specific protein which composes them: amyloid beta protein (Aβ).

In the century since Alzheimer's discovery, researchers have continued to investigate both Aβ itself and its genesis in the hopes of better characterizing the progression of Alzheimer's Disease. As average life expectancies across the globe continue to rise, cases of AD and other forms of dementia rise as well. Current predictions suggest that the number of people suffering from dementia in the US is expected to rise to 16 million by 2050 from the current 4-5 million [1]. Although other proteins have also been linked to AD (prion protein, tau, etc.), the importance of Aβ in the development and pathology of the disease has been demonstrated in numerous studies [6, 7], leading to the development of the "Amyloid Cascade Hypothesis" proposed by Hardy and Selkoe [8]. Their hypothesis suggests that accumulation of Aβ in the brain is the primary driving force for development of AD, and that factors affecting the production of Aβ begin the "cascade" culminating in onset of the disease.

1.1 Genesis of Aβ Protein

Aβ, the individual protein which aggregates to form the plaques and fibrils identified by Alzheimer, is generated from a much longer peptide known as Amyloid Precursor Protein (APP) [9]. APP is a Type 1 transmembrane (TM) peptide commonly found as a 770-residue sequence [10], although other forms have been studied consisting of different chain lengths [9, 11]. APP undergoes multiple sequential cleavage events to generate the final product [12], and can be processed along two known pathways: the amyloidogenic (which generates Aβ) and non-amyloidogenic pathways, both shown in Fig. 1.1.

In the non-amyloidogenic pathway, the initial cleavage event occurs extracellularly between residues K687 and L688 when APP is cleaved by the protein α-secretase. Since this α-cleavage occurs within the Aβ strand, this pathway inhibits formation of Aβ protein and instead generates the shorter, non-toxic p53 protein [13, 14].

In the amyloidogenic pathway - leading to the development of Aβ - the initial cleavage occurs at the N-terminus of Aβ: residue 672 on the APP strand. This process is performed by β-secretase and releases a large extracellular portion of APP (sAPP: soluble APP), leaving behind a 99-residue long membrane-bound fragment of APP called C99 [15, 16, 17]. This fragment then undergoes cleavage inside the lipid membrane by a large protein complex: γ-secretase [18, 19, 20], which generates Aβ and releases the Amyloid intracellular domain (AICD).

In the early 2000's, it was discovered that the γ-secretase cleavage pathway consists of multiple cleavage events, beginning at the C-terminal end of the TM domain, and progressing up the TM helix until a final cleavage event releases the Aβ peptide. The initial site of cleavage, named the ϵ-site, was discovered to most commonly occur between residues 49 and 50 on the C99 peptide [21, 22, 23, 24]. Subsequently, another cleavage location, the ζ-site was discovered further up the TM helix [25, 26, 27], and the sequential nature of γ-cleavage was further demonstrated [28, 29]. Two predominant pathways are currently known to exist (Fig. 1.2, resulting in the generation of a 40-residue peptide:Aβ_{1-40} and

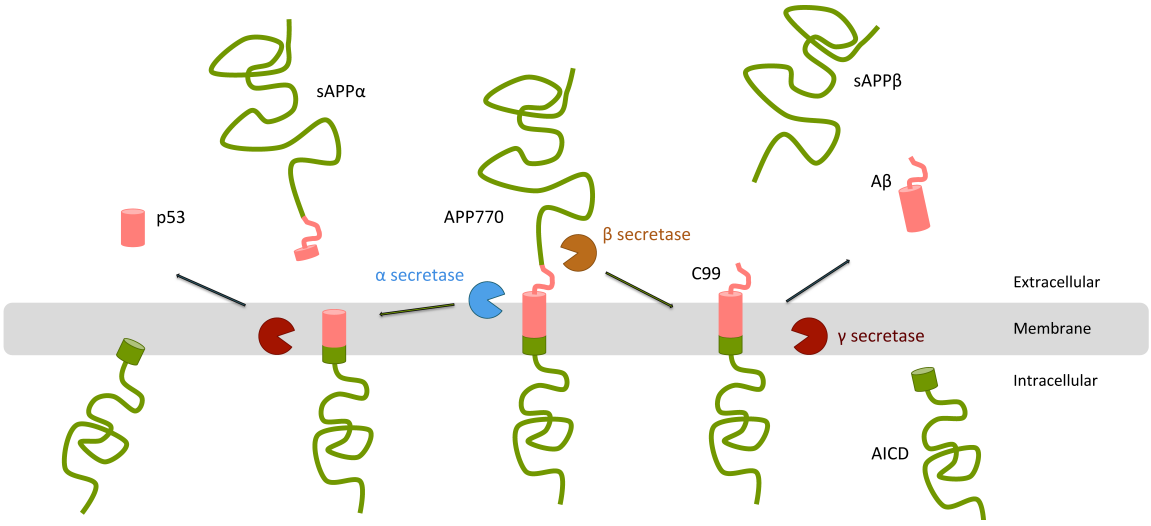

Figure 1.1: The two main processing pathways of APP. Left: an initial cleavage by α-secretase generates extracellular sAPPα, and subsequent processing by γ-secretase releases the non-amyloidogenic p53 peptide and AICD. Right: initial cleavage by β-secretase releases extracellular sAPPβ leaving behind the C99 peptide, which gets cleaved by γ-secretase to produce AICD and Aβ peptide.

a 42-residue peptide: Aβ_{1-42}, respectively. In the first, initial ϵ-cleavage at residue 49 is followed by ζ-cleavage at residue 46, and γ-cleavages at residues 43 and 40. In the second pathway, ϵ-cleavage begins at residue 48, proceeds to ζ-cleavage at residue 45, followed by γ-cleavage at residues 42 and possibly 38.

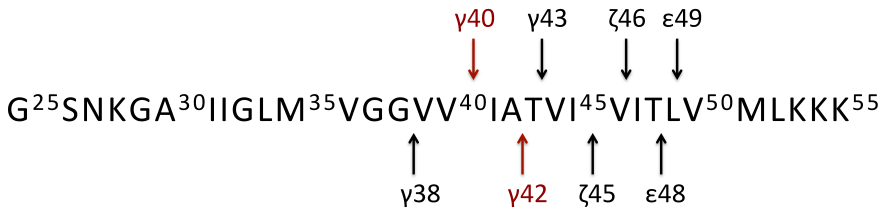

Figure 1.2: The main cleavage sites along the APP strand leading to Aβ_{1-40} (*top*) and Aβ_{1-42} (*bottom*).

This variable secondary cleavage event is the crucial part of the process, since it can result in a range of Aβ isoforms [30]. Aβ_{1-40} is the predominant form of Aβ, and is also the least neurotoxic. The resulting distribution of Aβ_{1-42} to Aβ_{1-40} is closely linked

to the development of AD. Changes in this ratio are correlated with the development of the characteristic plaques and fibrils as well as with the onset of dementia [31, 32]. For this reason, a better understanding of the cleavage of C99 by γ-secretase is crucial to characterizing the early pathogenesis of AD.

1.2 Dependence on Membrane Environment

A crucial aspect of Aβ genesis is that γ-cleavage takes place inside the lipid membrane. γ-secretase is part of a class of proteins known as iCLIPS, intramembrane cleaving proteases [33, 34, 35]. The active site is buried within the membrane, and cleavage actually occurs in the hydrophobic interior. This presents many challenges to experimental work, since resolving the structure of either APP or γ-secretase while inserted into lipids is difficult, and it makes it harder to probe the cleavage event by many standard means.

It also makes APP cleavage an interesting problem to study, since the exact mechanism of cleavage for many iCLIPS remains unknown. γ-secretase is known to be an aspartyl protease, yet it remains to be proven how the cleavage proceeds, and how water - a crucial part of aspartyl cleavage - accesses the active site for cleavage to proceed.

In addition to the interesting questions raised by the location of the active site in γ-secretase, the lipid environment has also been shown to play a crucial role in the structure and positioning of APP in the membrane [36], and that changes to the environment can affect the processing of APP [37]. Also, it has been shown that the presence of other factors in lipids, like cholesterol, can affect processing of APP and are linked to the development of AD [38, 39], although it remains unclear whether this happens solely because of changes to the environment, whether cholesterol interacts directly with APP to affect processing, or both. This means that gaining a better understanding of how APP relies on local environment could be crucial to understanding the genesis of Aβ and factors affecting the cleavage process.

1.3 Sequence

The genetic contribution to AD raises many interesting questions [2]. There are a number of known single-site mutations associated with Alzheimer's development or early onset of the disease. While some of these mutations occur on Presenilin 1 (PS1), the subunit of γ-secretase containing the active site, many have also been characterized on the APP strand itself. The location of these mutations vary, suggesting differing effects which lead to either increased chance or early onset of AD.

The earliest identified Familial Alzheimer's Disease (FAD) mutations were a set of mutations occurring at residue V46 (Aβ numbering). These "London" mutations included V46I/L/F/G [40, 41, 42]. One important characteristic of these mutations, and others which were later discovered in the three preceding residues, was that the mutations themselves were located beyond the C-terminus of the Aβ-protein sequence, indicating that the mutations were likely to affect processing of APP as opposed to affecting strictly the properties of Aβ itself. Similarly, following identification of the London mutants, two residues located immediately preceding the N-terminus of the Aβ sequence were identified as the location of the "Swedish" variants of FAD mutations: K670N/M671L (APP-770 numbering)[43]. Again, the location of the mutations outside the Aβ strand, and at the site of β-cleavage, suggested an influence on APP processing.

Subsequently a cluster of mutations was identified near the center of the Aβ strand including the "Flemish" (A21G) and "Dutch" (E22Q) mutants [44, 45]. Due to their location, these mutations could affect the processing of APP or the structure and aggregation of Aβ post-cleavage by γ-secretase, or possibly some combination of both effects. The Flemish mutant, in particular, presented with cerebral haemorrhage which has not been correlated to other FAD mutants, suggesting a different mechanism for the pathology of the A21G substitution [44].

In addition to characterized FAD mutations, many studies have also focused on "engineered" mutations which aren't known to be naturally occurring or genetically linked.

These mutations are designed to test specific hypotheses about the structure, positioning, and processing of APP by altering key residues in order to interfere with specific interactions or properties of the peptide. Many studies with engineered mutants have been instrumental in developing a more detailed understanding of the role each residue plays, and their importance in the genesis of Aβ protein [46, 47, 48, 49, 50].

1.4 APP Dimerization

Numerous studies have suggested that APP homodimerizes *in vivo* [51, 52, 53]. The exact role of dimerization in the processing of APP by γ-secretase has yet to be established, with some studies suggesting that dimerization might be a crucial step in the γ-pathway [54, 29] while others suggest that dimerization inhibits processing [55].

One factor suggesting that dimerization might be important to the etiology of APP processing is the existence of an extended GxxxG repeat motif in the sequence of the protein [54]. These GxxxG motifs are known to enhance dimerization of TM α-helices, promoting close right-handed coiled-coil packing [56]. This has especially been demonstrated in the Glycophorin A (GpA) compound. In the wild type (WT) APP sequence there are three sequential GxxxG repeats occurring from residue G25 to residue G37 [9].

The presence of these motifs suggests that dimerization of APP strands could play a crucial role in the processing of APP to produce Aβ protein. The existence of a specific interface enhanced by close-packing motifs might promote specific interactions between APP and PS1 when being cleaved by γ-secretase. If the motifs on two interacting APP strands were to interact during dimerization, it would promote a certain side of the APP TM-helix being made available for processing opposite the dimer interface. One convenient aspect of this theory is that the change in the cleavage site for Aβ_{1-40} and Aβ_{1-42} is two amino acids - or half of a helical turn. If dimerization is a component of APP processing, factors affecting the interface between dimers would alter which "face" of the TM-helix is available for γ-cleavage, and potentially change the resultant length of Aβ produced.

The role of APP dimerization remains contested. Certain studies suggest that homodimerization is crucial to APP processing [56, 51, 54], which others propose an inhibitory effect [55]. Although the specific mechanism of APP dimerization in the γ-processing pathway is not yet known, it remains an important characteristic of the APP system, and providing a better understanding of dimer interactions may help elucidate the nature of the specific role it plays in the genesis of Aβ.

Chapter 2

Methodology:

The sections in this chapter describe the general approach used to build the systems and run any simulations. Any differences between individual systems are noted in the following chapters.

2.1 Multiscale Approach

We employed a multiscale computational approach, combining molecular dynamics (MD) and replica exchange MD (REMD) simulations [57], using models including (1) all-atom representations of the protein in an implicit GBSW membrane [58], (2) coarse-grained models of the protein, lipids, and solvent using the MARTINI force field [59, 60], and (3) all-atom CHARMM36 force field models for the protein, membrane, and solvent environments [61, 62, 63, 64]. Representations of the varying levels of resolution are shown in Fig. 2.1. Chapters 4 and 5 employed all three levels of simulation, while chapters 3 and 6 only employed levels (1) and (3).

In the first stage, REMD simulations of an all-atom model of the protein in an implicit membrane allow us to explore the protein conformational ensemble. From those simulations protein conformations representative of important substates composing the overall ensemble were derived. These conformations were used to parameterize coarse-grained MARTINI force field simulations of the proteins in a particle model of the phospholipid bilayer. Coarse-grained simulations were used to assess the role of fluctuations in membrane thickness, explicit interactions between protein and head groups, interactions due to packing disorder in the lipid tail groups, and lipid composition of the membrane on the protein conformational ensemble. Subsequently, all-atom molecular dynamics simulations were used to refine key substates identified in the CG simulations and characterize the detailed

peptide-peptide, peptide-lipid, and peptide-solvent interactions. Results derived at varying levels of resolution were tested for consistency. This approach leads to enhanced sampling of the homodimer ensemble while simultaneously providing a detailed atomic-level picture of the $C99_{15-55}$ homodimer ensemble and its dependence on the bilayer environment [65, 66].

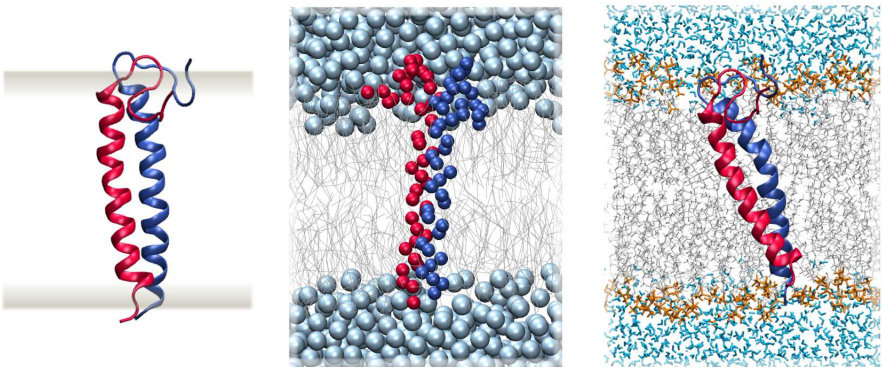

Figure 2.1: Depiction of the $C99_{15-55}$ dimer system at varying levels of resolution used in the multiscale modeling approach. Implicit membrane model (left), Martini (CG) model (middle) and all-atom model (right).

2.2 APP Fragments: Starting Structures

For simulations of full-length $C99_{1-55}$, the initial structure was generated by combining structural data from previous simulations of $A\beta_{1-40}$ along with a helical segment through residue 55 in the sequence. Structures for the $C99_{15-55}$ systems were taken from NMR-derived structures of $C99_{15-55}$ determined experimentally in DPC micelles, without the inclusion of the caps used in that study [67]. Structures for $C99_{23-55}$ were generated to be helical. All systems, regardless of length or sequence, were generated with the protein or dimer strands located in the center of the bilayer environment, along the membrane normal.

Structures for all-atom simulations were selected from completed replica-exchange molecular dynamics (REMD) [57] simulations of the desired systems. The number of frames used varied for each system dependent on relevant structural features or ensembles of interest.

Mutations were introduced to the proteins using the VMD software package [68], and mutant strands were minimized in CHARMM before beginning equilibration and production runs.

2.3 REMD Simulations

All REMD simulations were performed in CHARMM [69], with an all-atom model of the protein, and implicit representation of the solvent and membrane environments. The implicit model used was the Generalized Born model with a switching function (GBSW) [58], as implemented in CHARMM. This model uses a switching function at dielectric boundaries, and also models the head group regions of a membrane slab using a switching function to provide a smooth change between the solvent region and the membrane interior. Interiors were set to a dielectric value of 1, while the solvent region was set to a dielectric value of 80.

Proteins were modeled using the CHARMM PARAM22 force field with dihedral cross-term corrections (CMAP) [70], and with corrections specific for the GBSW model. Updated atomic radii for the GBSW model were also used [71]. The smoothing length used at dielectric boundaries was 0.6 Å, with 24 radial integration points, and no cutoff. The surface tension coefficient was set to 0.04 kcal/(mol $\cdot$ Å^2). The membrane was defined as a continuous slab in the xy plane, with the membrane normal lying along the z-axis. The timestep used for MD steps was 2 fs, and exchanges between neighboring replicas were attempted every 0.5 ps. Replicas were maintained using the MMTSB tool set [72]

2.4 All-Atom Simulations

Structures were inserted in pre-equilibrated POPC bilayers using the CHARMM-GUI [73, 74, 75]. All-atom simulations were carried out in GROMACS [76, 77]. After the initial structures were embedded in the bilayer, all structures underwent steepest descent minimization, followed by 100 ps of NVT and 2 ns of NPT equilibration. Each structure was

then simulated for 100 ns, with the initial 50 ns excluded from analysis.

Explicit all-atom simulations were performed using the CHARMM36 force field and TIP3P water atoms with a time step of 2 fs [78, 79]. PME was used to calculate long-range electrostatics, and short range electrostatics had a cut-off at 1.0 nm. A Nosé-Hoover thermostat was used along with a Parrinello-Rahman barostat to control the temperature and pressure [80]. The POPC bilayer consisted of 128 lipid molecules (64 each on the top and bottom layers), and the system was completed with TIP3P water molecules extending 20 Å on each side of the bilayer, and any necessary counter-ions to provide a neutral system.

Chapter 3

Engineered mutations to residue K28 affect the structure and positioning of APP-C99 peptide in lipid bilayer

3.1 Introduction

Alzheimer's Disease (AD) is currently the leading cause of dementia worldwide, and is estimated to be responsible for more than 65% of late-life dementia cases [1]. The amyloid β (Aβ) hypothesis suggests that the Aβ protein plays a critical role as a pathogenic agent in AD [8, 81]. The characteristic plaques and tangles associated with AD were first discovered by Aloys Alzheimer in 1906 [1], and in 1963 the individual protein itself, Aβ, was first identified [3]. Despite decades of research since that time, however, many questions remain surrounding the specific causes of not only the neurotoxicity of Aβ, but also the precise mechanisms controlling its genesis. The Aβ protein itself is a natural byproduct of regular cell functions, resulting from the cleavage of amyloid precursor protein (APP) [12, 14]. In its most common form, it exists as a 40-residue long peptide (Aβ40) predominant in cerebrospinal fluid and plasma [81]. Various isoforms of Aβ can result, however, and amyloid plaques in patients with AD are enriched with a slightly longer 42-residue peptide (Aβ42). Aβ40 and Aβ42 have been shown to exhibit different aggregation patterns [32], oligomer structures [31], and toxicity levels [82].

APP is a type I transmembrane protein which exists in isoforms ranging from 365 amino acids to the most common isoform of 770 amino acids [14, 7]. It can undergo two separate cleavage pathways; in the non-amyloidogenic pathway, APP is first cleaved by α-secretase [83, 13] then by γ-secretase [20], yielding the N-terminally truncated p53 peptide. In the alternate amyloidogenic pathway, β-secretase [17] cleaves at the N-terminus of Aβ yielding the membrane-bound APP-C99 fragment which may then be cleaved by γ-secretase

to yield Aβ. Cleavage of APP-C99 by γ-secretase is known to occur by sequential proteolytic events beginning at the ϵ-site (commonly Leu^{49}-Met^{50}), and proceeding to the final - variable - γ-site, which determines the isoform of Aβ generated [27, 25, 26].

There are many single-site mutations, both familial [84, 85, 86] and engineered [48, 87], which are known to affect the initial location or progression of these sequential cleavage events, and therefore alter the ratio of isoform distributions of Aβ. Many of these mutations, especially the familial mutants, are located in the region of the protein where the sequential cleavage events occur: residues Thr^{43}-Val^{46}. However, some mutations have also been studied which are located at the opposite end of the membrane, far removed from the actual location of cleavage, and yet have marked effects on the resulting isoforms of Aβ. One focus of study has been on the role of Lys^{28}, where engineered mutations have been shown to affect the length of the isoforms produced after γ-cleavage [46, 47, 48, 49, 50]. Although the exact mechanism of this change in the cleavage location is not yet known, studying the effects of mutations at this critical location in the APP sequence will help gain a deeper understanding of the genesis of Aβ.

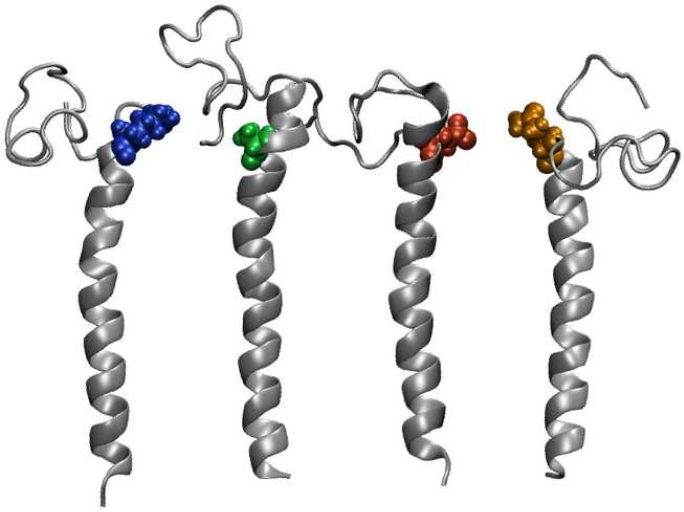

Figure 3.1: Four different C99$_{1-55}$ systems highlighting location of residue 28 for all sequences studied: Wild-type (blue), K28A (green), K28E (red), K28Q (orange).

This study examines the mutant systems analyzed by Kukar and coworkers (K28A,

K28Q) [48], as well as the often-investigated K28E mutation [47, 49, 50], in the hopes of providing an atomic-level view of changes caused by these specific single-site mutations (Fig. 3.1). Mutations at Lys^{28} have resulted in a variety of effects on the processing of APP. K28S mutation has been shown to cause almost a 90% decrease in Aβ production [46], while the K28E mutation causes a less drastic reduction in Aβ40 and Aβ42 amounts accompanied by an increase in the shorter Aβ37 and Aβ38 peptides [47, 49, 50]. The K28A and K28Q mutants have also been shown to increase production of shorter Aβ isoforms at the expense of Aβ40, especially in the case of K28A mutation, which nearly abolishes production of any Aβ isoforms longer than 34 residues [48, 50].

In order to reduce the system size and focus study on the transmembrane domain (TMD) of the protein, the first 55 residues of the full APP-C99 strand were used. This fragment (which we refer to as $C99_{1-55}$) comprises the entire Aβ strand as well as the following 15 residues of APP-C99. It extends through the TMD, and ends in three terminal Lys residues, providing a stable anchor to ensure that the protein remains embedded in the membrane as full-length APP-C99 would. Using a multiscale approach of implicit replica-exchange and all-atom simulations, the conformational changes and membrane interactions of these systems were analyzed and compared to experimental results to provide a more detailed understanding of the genesis of the Aβ protein in $C99_{1-55}$. Structural changes induced by sequence variation are characterized in terms of TM helix tilt and depth of insertions, as well as the stability of the TM helix, which has been studied for its effect on cleavage efficiency [36, 29]. These structural changes were found to be correlated with the impact on processing by γ-secretase. These observations provide a foundation for the formation of structure-activity relations (SAR) describing the impact of C99 mutation to the production of Aβ.

3.2 Methods

3.2.1 Multiscale Simulation

In order to adequately sample the entire structural ensemble of each system while also being able to investigate detailed interactions between the proteins and the environment, a "multiscale" approach was used consisting of two different levels of simulation. First, structures were simulated using the replica-exchange molecular dynamics (REMD) [57] method in order to increase conformational sampling. In REMD simulations, noninteracting replicas are each started at different temperatures, and regular MD steps are carried out at each temperature. At exchange steps, neighboring replicas have a chance to exchange temperatures according to the Metropolis criterion. This allows the replicas to diffuse across temperatures, and escape any local minima while sampling the conformational space.

Once REMD simulation was completed, the resulting structural ensembles for each peptide were investigated and clustered into relevant local minima in order to draw starting structures for explicit all-atom simulation. The explicit simulation allowed for more specific investigation of interactions between the proteins and the surrounding lipids and water molecules, without the approximations of the implicit environment. Once the all-atom simulations were completed, the two predominant structures for each peptide sequence were selected and used for analysis.

3.2.2 Initial Structures and Mutations

The initial structure used for the wild-type strand was built by generating a helical structure for the 55-residue sequence:

$$\mathrm{DAEFR^{5}HDSGY^{10}EVHHQ^{15}KLVFF^{20}AEDVG^{25}SN\mathbf{K}GA^{30}}$$
$$\mathrm{IIGLM^{35}VGGVV^{40}IATVI^{45}VITLV^{50}MLKKK^{55}}$$

The positions for the first 12 residues of the sequence were then replaced with the positions from a previous simulation of the Aβ40 protein, while remaining residues were kept in a

helical configuration. The new structure was minimized and oriented with respect to the membrane, so that the peptide was aligned along the membrane normal. This configuration was used as the starting structure. In addition to the wild-type peptide, three single-site mutants were investigated: K28A, K28E, and K28Q, where the lysine at residue 28 (shown in bold) was replaced by alanine, glutamic acid, and glutamine, respectively. These four systems cover all four types of amino acids at residue 28. For the mutant strands, the point mutations were constructed in VMD [68], and the resulting peptides were again minimized in CHARMM before equilibration and production.

3.2.3 Simulation Parameters and Force Fields

For the REMD simulations, 24 replicas were used to span a temperature range from 300 to 650 K. The timestep used for MD steps was 2 fs, and exchanges between neighboring replicas were attempted every 0.5 ps. The total simulation time was 168 ns (10.5 ns for each replica), and the initial 1 ns of simulation time for each replica were thrown out to remove any dependence on the initial structure. Replicas were maintained using the MMTSB tool set [72]

All REMD simulations were performed in CHARMM, with an all-atom model of the protein, and implicit representation of the solvent and membrane environments. The implicit model used was the Generalized Born model with a switching function (GBSW) [58], as implemented in CHARMM [69]. This model uses a switching function at dielectric boundaries, and also models the head group regions of a membrane slab using a switching function to provide a smooth change between the solvent region and the membrane interior.

For implicit simulations, the proteins were modeled using the CHARMM PARAM22 force field with dihedral cross-term corrections (CMAP) [70], and with corrections specific for the GBSW model. Updated atomic radii for the GBSW model were also used. The smoothing length used at dielectric boundaries was 0.6 Å, with 24 radial integration points, and no cutoff. The surface tension coefficient was set to 0.04 kcal/(mol $\cdot$ Å^2). The membrane

was set to a total width of 40 Å, with 5 Å at each end defined as the "head group" switching region, leaving a total of 30 Å as the membrane interior, with a dielectric value of 1. The switching function for the head group region then varied from the interior value to the solvent region, with a dielectric value of 80. The membrane was defined as a continuous slab in the xy plane, with the membrane normal lying along the z-axis.

From the completed REMD simulations, representative frames were selected as "seed structures" for all-atom simulations performed in GROMACS [76, 77]. Structures were inserted in pre-equilibrated POPC bilayers using the CHARMM-GUI [73, 74, 75]. All structures underwent steepest descent minimization, followed by 100 ps of NVT and 2 ns of NPT equilibration. Each structure was then simulated for 100 ns, with the initial 50 ns excluded from analysis.

Explicit simulations were performed using the CHARMM36 protein and lipid force field, and the TIP3P water force field, with a time step of 2 fs [78, 79]. PME was used to calculate long-range electrostatics, and short range electrostatics had a cut-off at 1.0 nm. A Nosé-Hoover thermostat was used along with a Parrinello-Rahman barostat to control the temperature and pressure [80]. The seed structures from the REMD calculations were embedded into a POPC bilayer consisting of 128 lipid molecules (64 each on the top and bottom layers), and the system was completed with TIP3P water molecules extending 20 Å on each side of the bilayer, and any necessary counter-ions to provide a neutral system.

3.3 Results

3.3.1 Mutation of K28 impacts salt-bridge formation

The first step in the multiscale modeling approach was to perform REMD simulations of the wild-type and mutant $C99_{1-55}$ systems in an implicit GBSW membrane environment [58] to sample the configurational space for all sequences. The mutations at residue 28 had a strong impact on the structures sampled in each system, as well as on select intrapeptide

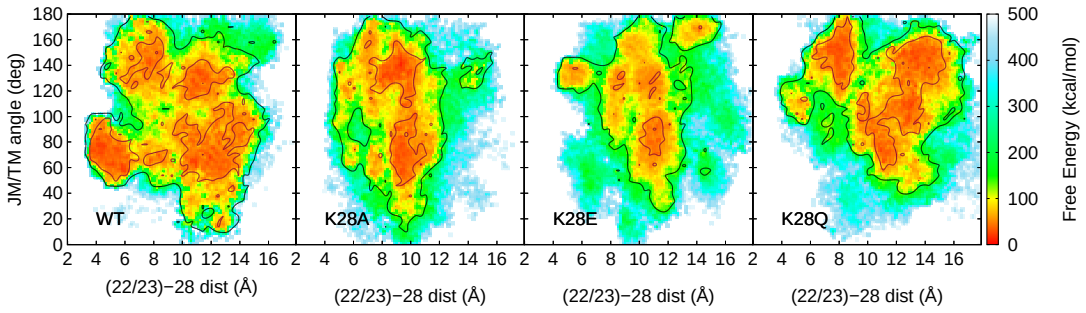

Figure 3.2: Conformational distributions of $C99_{1-55}$ in implicit membrane REMD simulations of all four $C99_{1-55}$ sequences, projected onto key order parameters (1) the salt-bridge distance between residues E22/D23 and residue 28 in each system and (2) the angle between the JM and TM regions of $C99_{1-55}$.

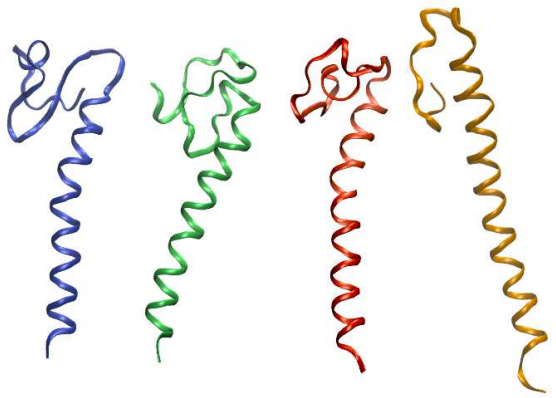

Figure 3.3: Representative structures of $C99_{1-55}$ in implicit membrane REMD simulations of all four $C99_{1-55}$ sequences, showing variety of structural ensembles. From left to right: WT (blue), K28A (green), K28E (red), K28Q (orange).

interactions. In order to characterize the ensembles for each system, the REMD results were analyzed along two main order parameters: the distance between residue 28 and residues E22/D23, and the angle between the juxtamembrane (JM) and TM regions. Fig. 3.2 shows the projection of the REMD simulations onto those order parameters.The differences in certain representative structures for each system can be seen in Fig. 3.3. The mutation has a clear effect on the variety of structures sampled, especially in the JM region of each peptide system.

In the wild-type sequence, K28 can form a salt bridge with the acidic E22/D23 residues

stabilizing a turn at the interfacial region of the protein. This salt-bridge interaction has been examined in studies of Aβ aggregation and found to promote a turn in the protein allowing for close β-interactions and packing between peptides to form fibrils [88, 89]. In the APP strand, however, this interaction occurs immediately N-terminal to the bilayer. The JM region of APP contains the sequence $L^{17}VFFA^{21}$, which is known as the central hydrophobic cluster (CHC) of Aβ. In the WT projection in Fig. 3.2, the cluster in the lower left of the plot is a region with close 22/23-28 interactions as well as a small angle between the JM/TM regions, suggesting that the salt-bridge facilitates reinsertion of the CHC into the bilayer. Changes to residue 28 appear to destabilize this interaction, and affect the positioning of the JM and TM regions relative to the membrane, as well as the structure of these regions. As seen in the mutant peptide projections in Fig. 3.2, the lower left cluster present in the WT peptide is absent in the mutant systems, although the K28E and K28Q systems both have a small cluster with a distance of around 6 Å, and a much larger JM/TM angle near 120-140 degrees.

3.3.2 Helix formation inhibits reinsertion of JM domain in POPC bilayer

Frames were selected from the predominant clusters for each system, and used to seed all-atom simulations in a POPC bilayer. When the simulations were analyzed, each $C99_{1-55}$ structural ensemble was found to be characterized by two principal structural forms, as shown in Fig. 3.4. In the wild-type strand, one cluster was characterized by structures having a stable JM-helix, which remained separate from the bilayer, while the other cluster featured structures with a β-strand formed from interactions between residues Q15 and F20, as was found in a recent structural study of $C99_{1-55}$ using FTIR spectroscopy [91]. In this second form, the CHC can be shown to reinsert into the POPC bilayer (Fig. 3.5).

In the WT peptide, the JM helix is composed entirely of the CHC residues ($K^{16}LVFFA^{21}$), in agreement with previous studies predicting the existence of a nascent JM helix [90, 67, 92]. This helix was also observed in the K28A and K28Q systems, while the K28E system formed

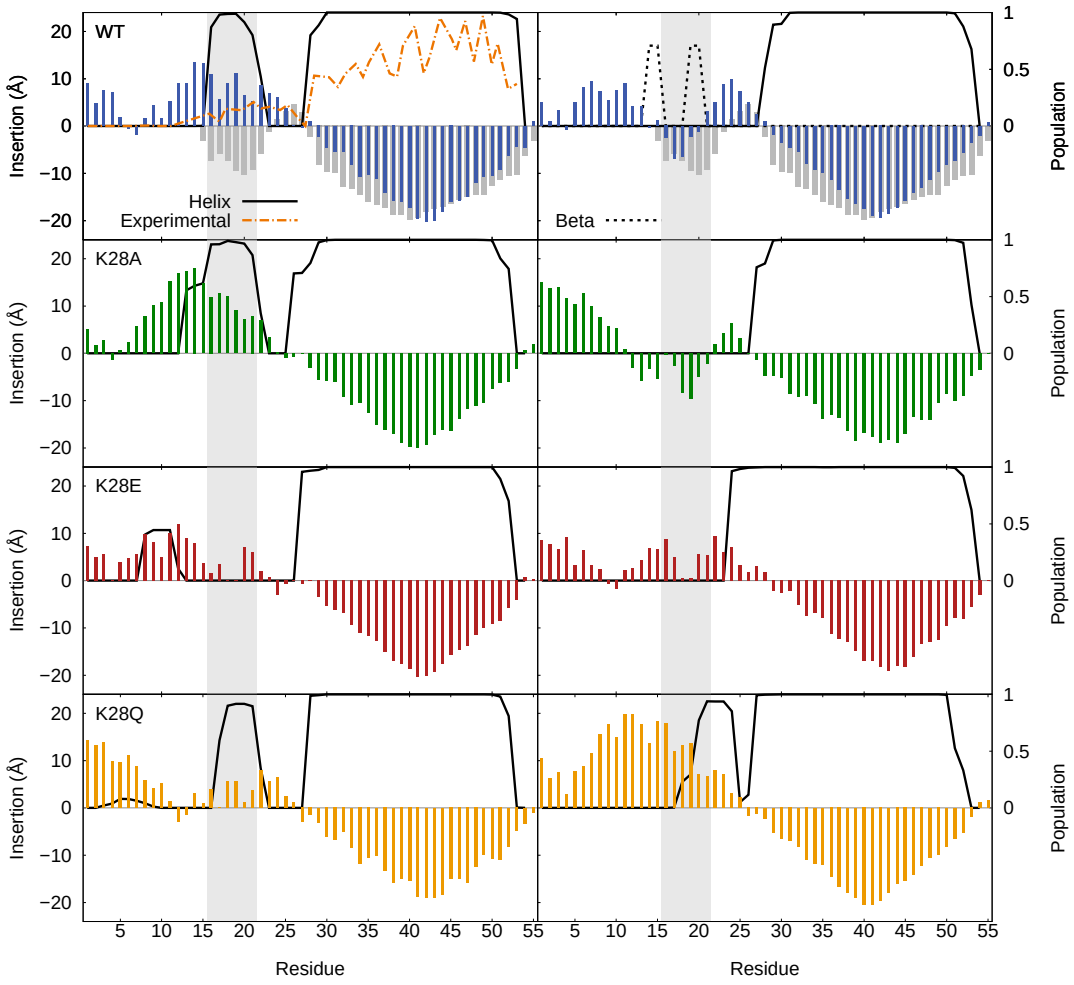

Figure 3.4: Distributions of $C99_{1-55}$ peptides in POPC bilayer derived from all-atom simulations, showing average location of each residue relative to the head-group region of the bilayer (colored bars), helix population (black line), and β-structure (dashed line). Negative values indicate insertion into the membrane. Experimental power saturation EPR measurements (gray bars) [90]. The orange dashed line overlaid on the WT data indicates helicity values calculated from C_α chemical shift NMR data [67]. Shaded gray area marks CHC.

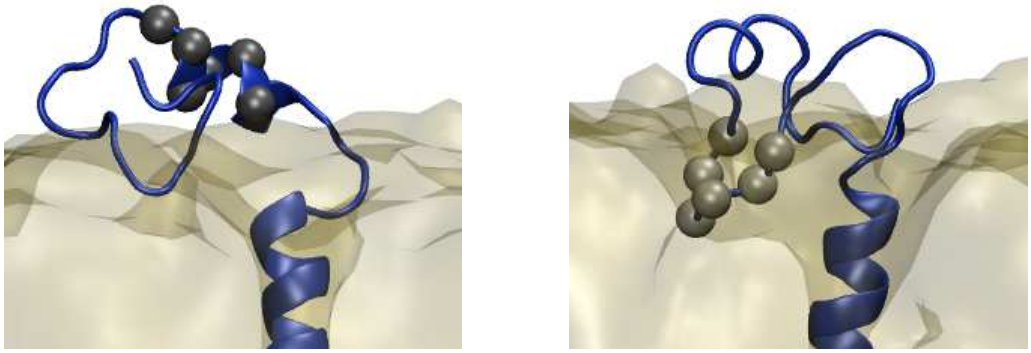

Figure 3.5: Characteristic structures of two dominant conformations of the WT peptide derived from all-atom simulations in POPC bilayer: (a) Helical JM region localized at the bilayer interface or (b) CHC region inserted in the lipid bilayer. Grey beads show the location of residues $K^{16}LVFFA^{21}$, and lipid domain is marked as a translucent surface.

a helix N-terminal to this location on the strand at residues $S^{8}GYE^{11}$. The reinsertion of the CHC into the bilayer was observed in all systems except the K28Q peptide, and only occurs in the absence of any JM helical content for the mutant systems as well as the WT peptide. This region of reinsertion has been previously reported for $C99_{1-55}$ in surfactant micelles [67].

3.3.3 Reorganization of JM domain in mutant forms of $C99_{1-55}$

To investigate the effect of mutation on the salt-bridge interaction, the distances between residue E22-28 and D23-28 were calculated independently from all-atom simulations of $C99_{1-55}$ in POPC bilayer as shown in Fig. 3.4. The results of this calculation are shown in Fig. 3.6. Distances between residues were calculated between the terminal portions of each amino acid (e.g. the carboxyl group on acidic residues, or the terminal methyl group on the alanine residue). Similarities can be seen for structures containing a helical CHC region in the WT, K28A, and K28Q systems, where there is an intermediate distance (∼5-10 Å) between residues 23 and 28, and a larger distance (∼15-20 Å) between residues 22 and

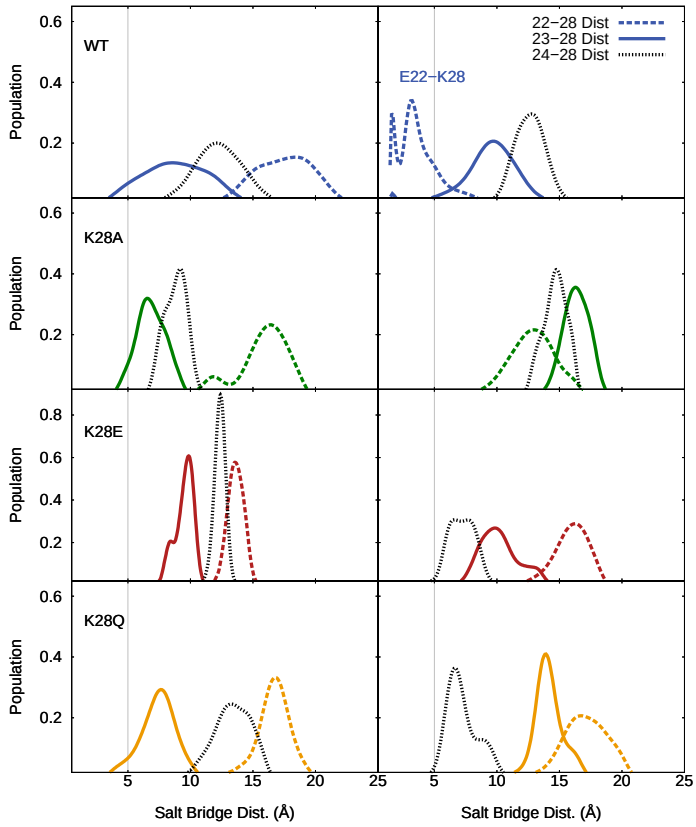

Figure 3.6: Residue pair distributions for $C99_{1-55}$ in POPC bilayer derived from all-atom simulations. Shown are normalized distributions for the 22-28 distance (dashed colored lines); 23-28 distance (solid colored lines), and 24-28 distance (dashed black lines).

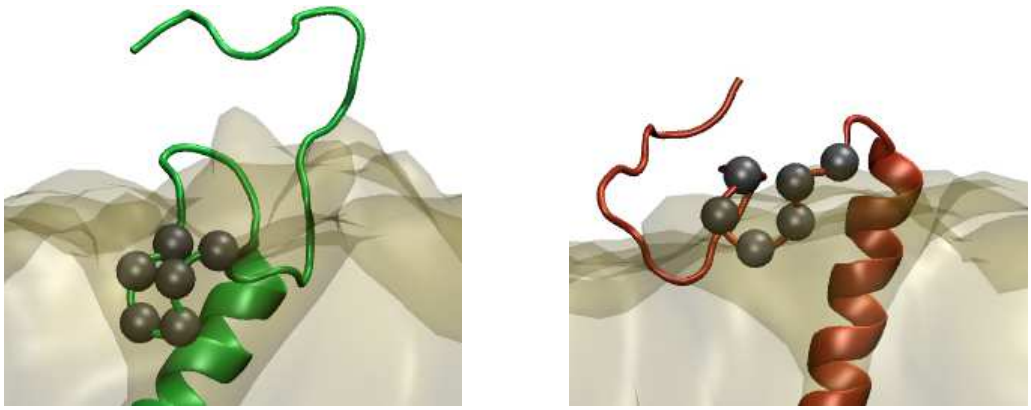

Figure 3.7: Characteristic structures derived from all-atom simulations in POPC bilayer showing reinsertion of the CHC region of the (left) K28A mutant peptide and (right) K28E mutant peptide. Grey beads show the location of CHC residues $K^{16}LVFFA^{21}$, and lipid domain is marked by the translucent surface.

28. In the K28E mutant, where interactions between residues 22/23 and residue 28 involve acidic residues in close proximity, neither of the two main structures show close contact interactions observed in the WT, K28A, and K28Q systems. Destabilization of this critical contact may account for the loss of helicity in the CHC region of the K28E peptide.

While structures with a helical CHC region have similar interactions between residues 23 and 28, interactions leading to reinsertion of the CHC region into the bilayer are more varied between systems. In the WT peptide, Fig. 3.6 shows a close salt-bridge formed between residues E22 and K28. Both the K28A and K28E systems, however, show little interaction between residue 28 and either of the acidic residues. Both systems, however, accommodate the change of those interactions in different ways. Whereas the WT structure with reinserted JM region adopts an "S"-like structure allowing reinsertion of the JM region, the K28A structure adopts a spiral "O"-like shape, establishing a greater distance between residues 22/23 and 28 (see Fig. 3.7, left). In the K28E structure (Fig. 3.7, right) the same "S"-bend is seen as in the WT, however, the TM-helix is extended toward the N-terminus (Fig. 3.4), which accounts for the observed changes in intrapeptide contacts.

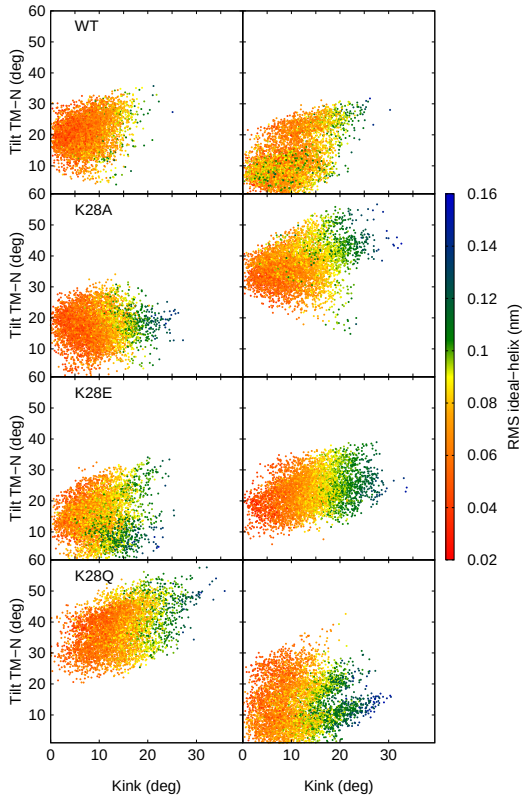

Figure 3.8: Distributions of kink and TM-helix tilt angles derived from all-atom simulations of $C99_{1-55}$ in POPC bilayer for each system. Coloring indicates RMS deviation from an ideal helix in nm over the TM domain.

3.3.4 Sequence-structure relations for TM domain of $C99_{1-55}$ in POPC bilayer

The point mutations studied also impact the position of the TM domain of $C99_{1-55}$. Fig. 3.8 shows the correlation of helix tilt and kink angles for the dominant clusters for each peptide system. Kink angles were calculated at residues G37/G38, with a value of 0 degrees indicating a straight TM helix. The TM angle was calculated for the N-terminal portion of the TM helix (up to residues G37/G38), and is given as a deviation from the membrane normal. Predominant structures in the WT system had smaller values for both the kink and tilt angles. Especially in the structure with a JM helix, the tilt relative to the membrane normal is below 30 degrees, with less than 15 degrees of kink in the helix. The reinserted

structure shows slightly larger kink angles (up to 20 degrees), but both structures deviate only slightly from an ideal helix.

The K28E mutant system shows similar positioning to the WT system, with both structures characterized by tilt values below 30 degrees. However, the reinserted structure shows no tilt values lower than 10 degrees, in contrast to the WT. The reinserted K28E structure is characterized by slightly larger kink values than the WT, which might result from the extended TM helix. In contrast to the WT and K28E peptides, both the K28A and K28Q mutant strands have structures that are less tilted featuring stable JM helices, and alternative structures with heavily tilted TM portions.

3.4 Discussion

3.4.1 WT C99$_{1-55}$ adopts two characteristic conformational states

The role of the JM region of C99 in the processing of APP by γ-secretase is currently unclear. Studies have found that mutations in this region can inhibit production of Aβ [93] as well as alter the resultant isoform distribution following γ-cleavage [46, 47, 48, 49, 50]. Structural studies of this region have suggested that the JM region may contain a moderately stable helical domain [92] that could play an important role in C99 homodimerization. The most-often reported structure found in that region was a nascent helix [67, 92, 90], but a recent study done using FTIR spectroscopy found evidence of β-structure in this region [91].

We find that the WT APP strand adopts two predominant conformational states, one featuring a helical JM domain, and the other stabilized by β interactions between residues Q15 and F20 (Fig. 3.4). These results agree with previous structural studies of APP suggesting that the WT JM structure might be inherently more flexible than the TM domain.

3.4.2 CHC helicity and bilayer insertion are distinct substates

Some studies have suggested that the CHC region of C99 forms a helix that is reinserted into the membrane [67, 92, 90]. In contrast, this study found that helicity in the CHC region is distinctly separate from structures where it is reinserted into the membrane bilayer. This was demonstrated across all four of the peptide systems investigated (Fig. 3.4). As seen in the WT, K28A, and K28Q systems, the formation of a JM-helix was correlated with extended JM structures localized near the bilayer interface. In contrast, when the CHC region reinserted into the membrane, no helical content was observed in the JM region.

Reinsertion of the CHC region was also found to be correlated with an increased peptide kink at the G37/G38 residues (Fig. 3.8). This suggests that reinsertion of the LVFFA residues of the CHC imposes a steric effect on the peptide requiring an increased kink to allow the turn at the interfacial region to form.

The two observed characteristic structures of the CHC region were associated with distinct intrapeptide interactions, especially in the WT system. In the structure containing a JM helix, the salt bridge formed between residues E22/D23 and K28 was much weaker and more diffuse, and featured stronger interactions involving D23 than E22. In the reinserted structure, the salt bridge was very well formed, and the interaction shifted to residue E22, which remained at distances of < 5Å from residue K28. This close salt bridge formation was not seen in any of the mutant systems, being destabilized by replacing the positive charge at residue 28, and might account for the loss of β-structure in the mutant peptides.

3.4.3 Mutations at residue K28 strongly affect peptide structural ensemble

All mutations studied had pronounced and distinct effects on the structural ensemble of the $C99_{1-55}$ peptide. Mutation of cationic K28 to polar (K28Q), non-polar (K28A), and acidic (K28E) residues destabilized the strong salt bridge capable of forming in the WT. While this interaction stabilizes the β-interaction allowing for reinsertion in the WT peptide, the

K28A and K28E systems both adjusted to allow for reinsertion in differing ways.

In the K28A system, the peptide adopted a strongly kinked and tilted structure, which positioned the N-terminal region of the TM domain at a sharp angle relative to the membrane normal (Fig. 3.8). This structure satisfied the steric requirements to allow reinsertion of the CHC without formation of the E22/K28 salt bridge. The K28E system, in contrast, avoided unfavorable acid/acid interactions introduced by mutation by extending the TM helix through residue V24. This structural feature can be seen both in Fig. 3.4 (K28E, right), as well as the close interaction between residues V24/E28 in Fig. 3.6, which arises from the two residues being one helical turn apart.

The K28Q system also adopted a more heavily kinked and tilted structure, similar to the K28A system (Fig. 3.8), but due to the increased stability of the JM helix in this peptide, little or no reinsertion of the CHC region was observed.

3.4.4 Possible effects of secondary structure and peptide position on processing by γ-secretase

Each of the mutations studied have been found to decrease production of Aβ_{1-40} in favor of shorter Aβ fragments [47, 48, 49, 50]. It was suggested when the luminal region of C99 was first investigated that the positive charge located at residue K28 might be necessary for normal processing by γ-secretase to occur [46]. Indeed, studies of the K28R mutant have shown cleavage patterns for the mutant peptide that are almost identical to WT C99 [46, 49, 50].

The positive charge of K28 appears to stabilize the salt bridge formation favoring β-structure, which, in this study, was only observed in the WT sequence, and was correlated with reinsertion of the CHC region. As suggested by Kukar *et al.*, for normal γ-cleavage to occur there might be a steric hindrance imposed by the JM region inhibiting the C99 strand from being more deeply inserted into the membrane to allow further sequential processing by γ-secretase. The interfacial turn and reinsertion of the CHC could provide that steric

barrier. One way this could be investigated in future studies would be to examine double mutants, where the K28E mutation would be combined with mutations at residues E22/D23 to recreate a salt bridge turn and potentially rescue normal γ-processing.

Another possible mechanism for mutations to affect the processing was presented by Ousson *et al.* suggesting that a change in membrane positioning or tilt could affect the locations of individual residues within the bilayer, allowing for further processing to generate shorter Aβ fragments [49]. This theory is also supported by our results, with the K28E strand (known to favor Aβ37 production) showing a slight increase in tilt, and the K28A/Q systems (both favoring shorter Aβ33/34 fragments) showing a dramatic increase in the N-terminal peptide tilt. Support for these two possible mechanisms helps provide more foundation on the SAR of the $C99_{1-55}$ peptide.

Other proposed theories involve specific interactions of the APP sequence with PS1 or other subunits of γ-secretase, which is beyond the scope of this work. These proposed mechanisms for JM mutations within the Aβ strand to affect and alter processing by γ-secretase must be critically evaluated in future studies.

Chapter 4

Transmembrane domain homodimer of Amyloid Precursor Protein adopts multiple conformational substates in lipid bilayers [1]

4.1 Introduction

Amyloid precursor protein (APP), a membrane-bound protein, is processed to release the amyloid-β (Aβ) peptide whose aggregation is linked to Alzheimer's Disease (AD). APP is known to undergo sequential cleavage, beginning with processing by β-secretase to release the 99 amino acid C-terminal fragment, APP-C99 (C99) [94], which is then processed by the γ-secretase complex starting at the C-terminal transmembrane (TM) helical region, and ending with the release of Aβ protein [28, 95, 96]. Many factors affect γ-secretase cleavage, including sequence [97, 54], TM helix stability [98, 36, 29], dimerization of C99 peptide [51, 53, 55, 99], as well as membrane composition [36].

Several studies of monomeric C99 have provided details of the peptide structure, particularly the TM helix. Early NMR structural studies of C99 in an LMPG micelle environment noted the existence of a flexible GG-kink in the TM helix near G37/G38 [90]. We had predicted the presence of such a kink using simulations of $C99_{1-55}$ in an implicit membrane environment [100], noting a flexible "hinge" at G37/G38 flanked by an N-terminal helix (Domain B) and C-terminal TM helix (Domain C), with Domain B showing larger fluctuations. These findings were in agreement with previous NMR studies [67]. We also discovered a third helical domain in the N-terminal juxtamembrane region (Domain A). A recent study involving H/D exchange experiments on the C99 peptide complemented with molecular dynamics simulations of $C99_{28-55}$ in a POPC bilayer also support this view of

[1] All coarse-grained and all-atom simulations and analysis in this chapter were performed by Dr. Laura Dominguez.

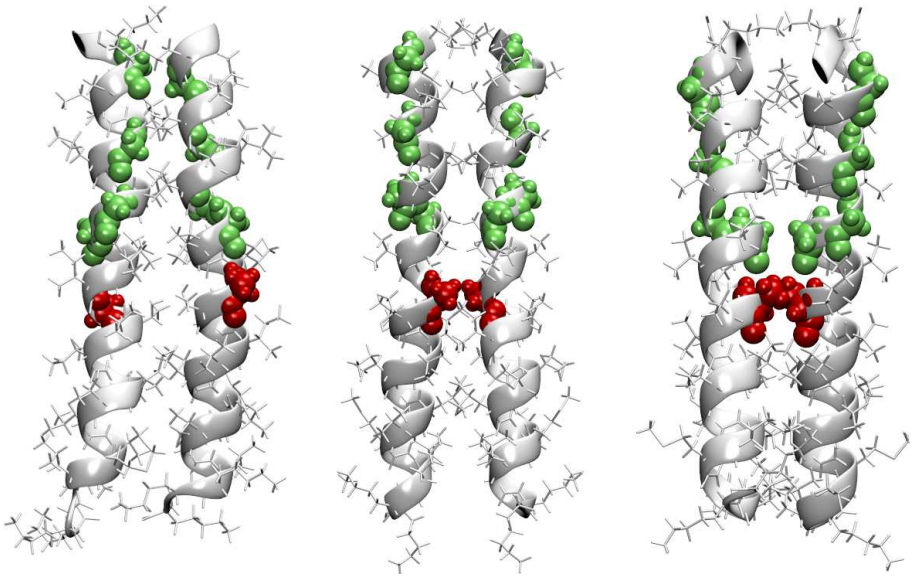

Figure 4.1: Different $C99_{15-55}$ dimer interfaces. Left: a $C99_{15-55}$ GxxxG motif at the interface and a right-handed crossing angle between the helices; Center: GxxxA motif at the interface with a right-handed crossing angle between the helices; Right: GxxxA interface with a left-handed crossing angle between the helices. Key Gly residues (G29, G33, G37 and G38) are shown in green and Ala 42 is shown in red.

the monomer structure consisting of three principal helical domains [29]. Thus, there is considerable agreement between theory and simulations regarding the structural ensemble of C99 monomer in membranes.

The earliest proposed structure for the C99 homodimer was inspired by sequence analysis, noting GxxxG repeats in the TM domain and homology with glycophorin A (GpA), in which GxxxG repeats facilitate interpeptide interactions stabilizing a right-handed coiled-coil homodimer [54]. Subsequent work supported this model, including NMR studies of C99 in a micelle environment [67]. In addition, the first simulations of the homodimer of $C99_{23-55}$ in a membrane environment [100] suggested a λ-like right-handed helical dimer structure stabilized by the GxxxG motifs, consistent with solid state NMR studies [98], as shown in Fig. 4.1 (left).

Subsequently, coarse-grained MD simulations refined by all-atom modeling provided

additional support for this model, while also noting the potential importance of interpeptide interactions mediated by the G38xxxA42 motif [101]. Further support for the importance of this secondary structural motif was provided in a subsequent study involving H/D exchange experiments on the C99 peptide complemented with molecular dynamics simulations of $C99_{28-55}$ in a POPC bilayer [29], as well as a model predicted by Monte Carlo searches of TM helix interactions [53].

Recently, the first experimentally-derived solution-phase structure of a homodimer of the TM domain of C99 in a detergent micelle was proposed, suggesting a dominant *X*-shaped left-handed coiled-coil structure stabilized by the GxxxA motif [92] (Fig. 4.1, right). Given past evidence based on mutation studies, NMR studies, and simulation suggesting a right-handed coiled-coil structure, this finding is a surprise [96, 100]. Another more recent structure also suggests a dominant GxxxA motif, but with the TM helices interacting in a right-handed orientation [102] (Fig. 4.1, center).

These differing views of the C99 homodimer structure raise important questions about the interactions of APP homodimers and their structure. How does the structure of C99 homodimers depend on sequence and lipid environment? What is the structure of the C99 homodimer in a biologically relevant membrane bilayer environment? How does dimerization of C99 influence its TM structure, helix stability, and availability to cleavage by γ-secretase?

Building on prior computational and experimental studies, we have explored the homodimerization of $C99_{15-55}$ in lipid bilayer environments using a multiscale modeling approach. Our simulations demonstrate that the $C99_{15-55}$ homodimer structure must be represented by multiple states, characterized by the relative orientations of the TM helices and stabilized by distinct intermolecular contacts. The relative probability of each substate is dependent on sequence and membrane environment. The most important implication of our finding is that the recognition and processing of the homodimer by γ-secretase is state-dependent, and that changes in the substate distribution may be reflected in the product distribution

of Aβ isoforms.

4.2 Methods

4.2.1 Choice of initial conditions

Initial conditions for the REMD simulations were taken from experimentally derived structures determined by NMR of $C99_{15-55}$ in DPC micelles (PDB 2LLM in the absence of the N-terminal caps) [67]. Monomer configurations were separated and randomly reoriented. To study $C99_{15-55}$ in POPC bilayer environment using both CG and all-atom models, initial conditions were derived from high probability structures observed in the REMD and CG ensembles, respectively. The POPC bilayer was generated using the CHARMM-GUI Membrane Builder [75, 74] and modeled using the CHARMM36 all-atom lipid force field and TIP3P water model [78, 79]. All systems included Cl^- ions to maintain electroneutrality.

To construct the CG peptide and bilayer systems, VMD [68] was used to overlap the coordinate files of the peptide and the pre-equilibrated lipid systems and delete the lipid and water residues within 1.5Å of the CG peptide. The pre-equilibrated boxes were taken from the Marrink website and definitions of all CG particles for the peptide were generated using the Martinize.py script with the MARTINI forcefield for proteins [103]. The CG parameters for lipids, ions, and W water molecules were as described in the MARTINI forcefield [59]. The protein transformations between CG and all-atom models were performed using Pulchra [104]. To study the self association of $C99_{15-55}$ dimers using a CG model, two $C99_{15-55}$ CG monomers were initially separated by 45Å in a system of POPC lipids and W waters. System sizes and sampling time scales are defined in Table 4.1.

4.2.2 Methods for simulation and analysis

The replica-exchange molecular dynamics (REMD) method was used in order to increase conformational sampling [105]. Simulations were performed in CHARMM [78], with an

Table 4.1: System sizes and time scales for implicit solvent, coarse-grained, and all-atom simulations.

Lipids	Waters	Force field	Time	Structure
256 POPC	3863 W	Martini 2.2	50 × 2μs	$C99_{15-55}$ + 45Å apart
Implicit	Implicit	CHARMM27+GBSW	24 × 10.5 ns	α-helix + 20Å apart
128 POPC	7176 TIP3P			Gly in (REMD)
128 POPC	7441 TIP3P	CHARMM36	100 ns	Gly out (CG)
128 POPC	7727 TIP3P			Gly side (REMD)

all-atom model of the protein and implicit representation of the solvent and membrane environments using the GBSW model [58]. The PARAM22 force field with the CMAP correction was used, including corrections specific for the GBSW model with updated radii [58]. The smoothing length used at dielectric boundaries was 0.6Å, with 24 radial integration points, and a cutoff of 20 Å. The surface tension coefficient was set to 0.04 kcal/mol Å. The membrane width was 42Å with a 10Å "head group" switching region at each end, leaving a 22Å width as the membrane interior. The switching function for the head group region varied from the interior dielectric constant value of 1 to the solvent region dielectric of 80. The membrane was defined as a continuous slab in the XY-plane, normal to the Z-axis.

CG simulations in POPC bilayer consisted of 50 replicas that were each simulated for 2 μs of "Martini time." Non-bonded interactions were truncated using shift functions (between 0.9 and 1.2 nm for Lennard-Jones interactions and between 0 and 1.2 nm for electrostatics) [59]. The temperature of the system was set to 303 K using the Berendsen weak coupling method [106] with a coupling time of 0.1 ps. An integration time step of 30 fs was used in all simulations. The pressure was set to 1 bar using a semi-isotropic coupling with the Berendsen algorithm.

All-atom simulations in the POPC bilayer consisted of 100 ns of MD performed on each all-atom system (following minimization and a short NVT and NPT equilibration with the protein backbone fixed). The non-bonded interactions were truncated using shift functions (between 0.9 and 1.2 nm for Lennard-Jones interactions and between 0 and 1.2 nm for electrostatics). Long-range electrostatic interactions were calculated using the Particle Mesh Ewald (PME) method [107] with a Fourier grid spacing of 0.12 nm. The pressure was set to 1

bar using a semi-isotropic coupling scheme with lateral and perpendicular pressures treated separately with coupling time 0.1 ps using the Parrinello-Rahman barostat methodology. The temperature of the system was set to 303 K and regulated using the Nosé-Hoover weak coupling algorithm [80]. The linear constraint solver (Lincs) method [108] was used to constrain all bond lengths, with a 2 fs integration step. The simulations were carried out using CHARMM [78] or GROMACS (v4.5.1). The analyses were performed using the CHARMM or GROMACS packages, the DSSP program, and tailored scripts using Python and MD Analysis libraries [76, 77, 109, 110, 111]. Images were generated using VMD [68]. All simulations were performed on the Boston University Katana and SSC supercomputers.

4.3 Results

We employed a multiscale modeling approach (see Fig. 2.1) by initially simulating $C99_{15-55}$ homodimer using REMD and an all-atom model of the peptide in an implicit Generalized Born with a simple Switching (GBSW) membrane environment. The membrane thickness was chosen to approximate the thickness of an all-atom POPC bilayer, with the end-to-end distance set to 42Å, and the center-to-center distance of the switching region set to 32Å. These simulations were used to derive structural ensembles for $C99_{15-55}$ homodimer that were analyzed in terms of depth-of-insertion, tilt angle, and peptide helicity.

The REMD results informed the parameterization of a MARTINI coarse-grained (CG) simulation model of the $C99_{15-55}$ homodimer for use in microsecond simulations of the $C99_{15-55}$ homodimer in a POPC (1-palmitoyl-2-oleoyl-sn-glycero-3-phosphocholine) lipid bilayer. The simulated conformational ensemble was analyzed in terms of the homodimer structure and the dependence on the membrane environment.

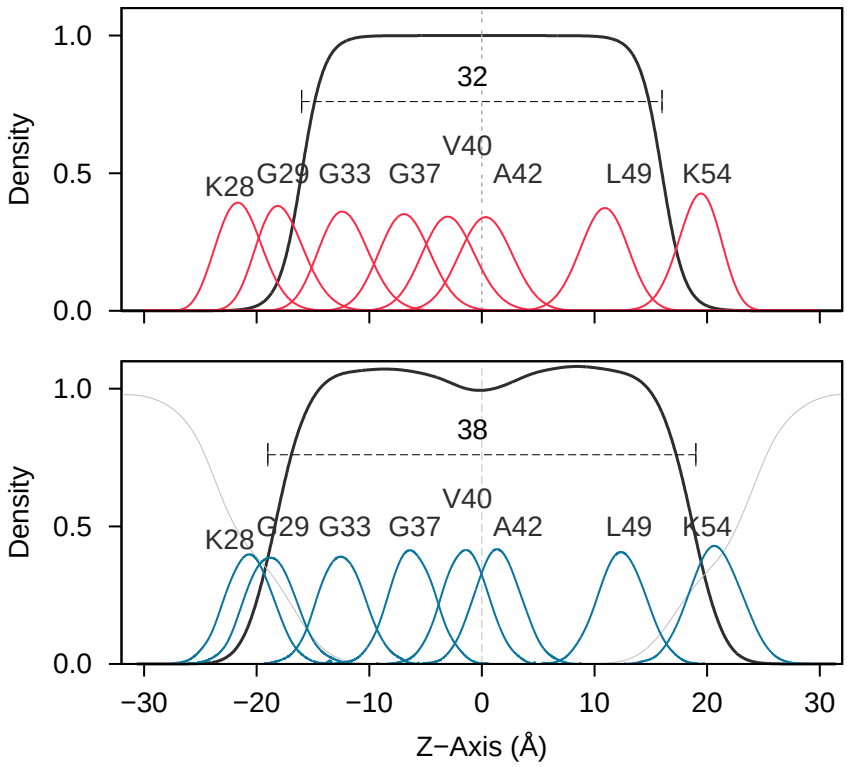

Figure 4.2: Lipid density profiles derived from REMD simulations using an all-atom CHARMM model of the peptides and implicit GBSW membrane model (upper) and CG Martini model MD simulations of the peptides in a POPC bilayer (lower). Dashed lines indicate the center-to-center distance of the switching region (GBSW simulation) or head group region (CG simulation) for each system.

4.3.1 C99$_{15-55}$ homodimer consists of two helical domains with distinct GG hinge in TM helix.

The computed lipid density profile and depth-of-insertion of key peptide residues for the CG POPC bilayer is presented in Fig. 4.2, in comparison with results derived for an all-atom peptide model in an implicit GBSW membrane model. The average width of the two membranes is similar, although the lipid density profile is found to be slightly broader and more diffuse in the CG particle model of the POPC bilayer. In spite of these differences in the membrane profiles, the distributions of depth-of-insertion for key residues of the peptides are quite similar in the implicit and CG models. This suggests that while the

interfacial regions are different in structure, the depth-of-insertion of the residues is largely determined by the tilt angle of the TM helix, which is largely determined by the average membrane thickness and is similar in both models.

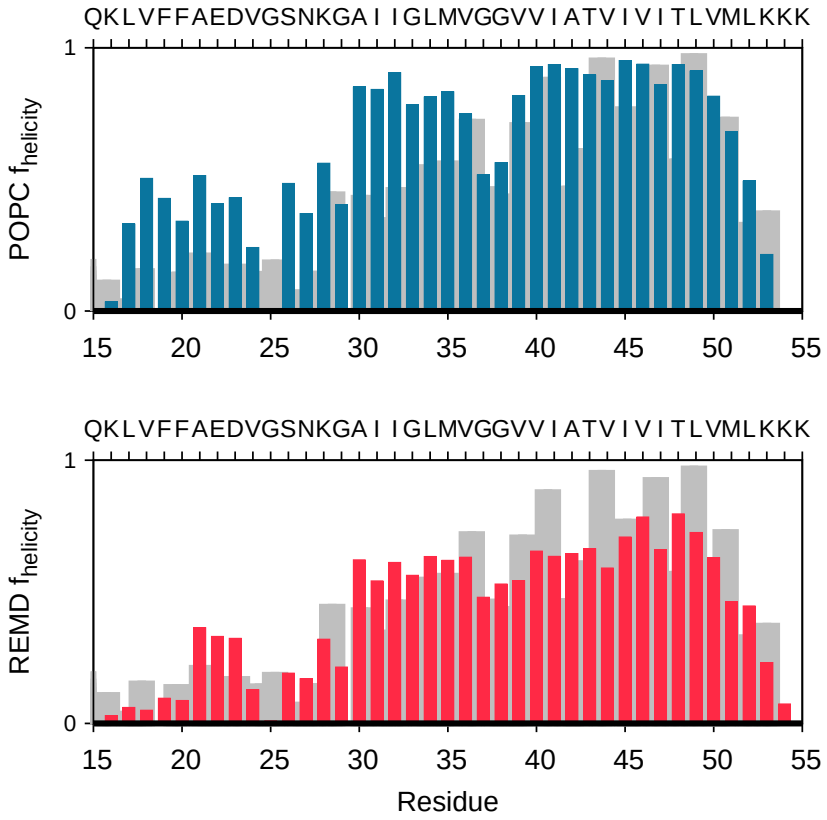

Figure 4.3: Helicity of peptides in the $C99_{15-55}$ homodimer ensemble simulated (top) using all-atom simulation in an explicit POPC bilayer, and (bottom) using REMD and an implicit GBSW membrane model. The grey shadow shows experimentally determined helicity based on C_α NMR chemical shift measurements for monomeric $C99_{1-55}$ in an LMPG (lysomyristoylphosphatidylglycerol) micelle [67].

The peptide helicity (see Fig. 4.3) derived from REMD simulations in an implicit membrane model is consistent with data published previously for $C99_{1-55}$ monomer in a similar implicit membrane model [100] as well as more recent all-atom simulations of $C99_{28-55}$ homodimer in a POPC bilayer [29]. The results show a clearly defined TM helical region, reduced helicity within the TM region near the dynamic GG hinge centered on G37/G38, and a distinct but less stable N-terminal JM helix. Interestingly, peptide helicity in the

simulated $C99_{15-55}$ homodimer is consistent with estimates derived from NMR studies of $C99_{15-55}$ monomer in an LMPG micelle. This suggests that homodimerization does not impact peptide helicity in agreement with previous results of NMR studies of $C99_{13-55}$ homodimer in detergent micelles [92].

4.3.2 Structural states of $(C99_{15-55})_2$ characterized by relative orientation of GxxxG repeat motifs.

Good order parameters for the homodimer structure are (1) dihedral angle ϕ_{4G} formed by $G29_A$-$G37_A$-$G37_B$-$G29_B$, where A and B label the two $C99_{15-55}$ monomers, and (2) interhelical distance d_{GG} between $G33_A$-$G33_B$. The ϕ_{4G} order parameter is positive for left-handed structures and negative for right-handed structures. Structures stabilized by interpeptide interactions facilitated by the GxxxG repeat region are characterized by small values of d_{GG}.

Peptide conformational distributions derived using REMD with an all-atom peptide potential and implicit GBSW membrane model as well as the CG MARTINI model are largely consistent for the two levels of modeling (see Fig. 4.4, top panels). In particular, both models lead to overall conformational ensembles consisting of close ($d_{GG} \approx 5$Å), intermediate ($d_{GG} \approx 10$Å), and longer-range d_{GG} interactions. Both models yield close d_{GG} interactions that can be right- or left-handed, but favor right-handed conformations. Also, both models show a range of intermediate d_{GG} values, including both right-handed and left-handed structures.

An additional valuable order parameter for the evaluation of interhelical contacts is the Crick angle, ψ_{Crick}, between (1) the vector connecting the axis points of the two helices and (2) the vector connecting C_α of a given residue to its corresponding α-helix axis point [112, 113, 114]. Smaller values (between 0 and 60) identify residues closer to the dimer interface, while larger angles (close to 180) denote residues on opposite sides of the interface. We define ψ_{Crick} to be the average of the G33 and G37 Crick angles in order to characterize

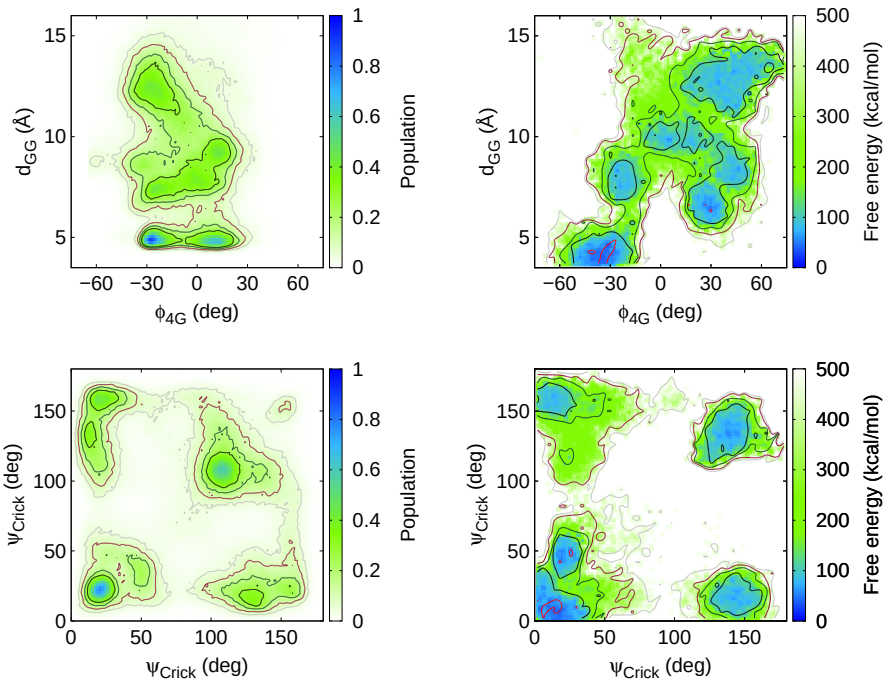

Figure 4.4: $C99_{15-55}$ homodimer populations derived from CG simulations with POPC membrane (left panels) and REMD simulations with implicit membrane (right panels) projected onto the order parameters ϕ_{4G} and d_{GG}. Upper panels show the d_{GG} - ϕ_{4G} values while lower panels depict projections onto ψ_{Crick} angles. Scales for all the graphs are on the right.

the G33xxxG37 interface.

The lower panels of Fig. 4.4 show projections onto the two peptide ψ_{Crick} angles. The symmetry of the distribution above and below the diagonal demonstrates the goodness of sampling achieved by both sets of simulations, as individual peptides forming the homodimer sample a similar range of conformations. The CG and implicit GBSW simulations sample dimer structures consisting of the GxxxG motifs on both peptides facing the interface (bottom left), both GxxxG motifs facing away from the interface (middle/top right), and structures where the GxxxG motif of one peptide faces the interpeptide interface and the other faces away (top left/bottom right). These distinct states can be characterized in detail in terms of the relative peptide orientations and interpeptide contacts.

4.3.3 $(C99_{15-55})_2$ structural ensemble consists of three distinct conformational states

The structural ensemble has a number of important characteristics. The predominant topology of the homodimer is a right-handed coiled-coil with three populated states which can be generally characterized in order of relative prominence (see Fig. 4.5).

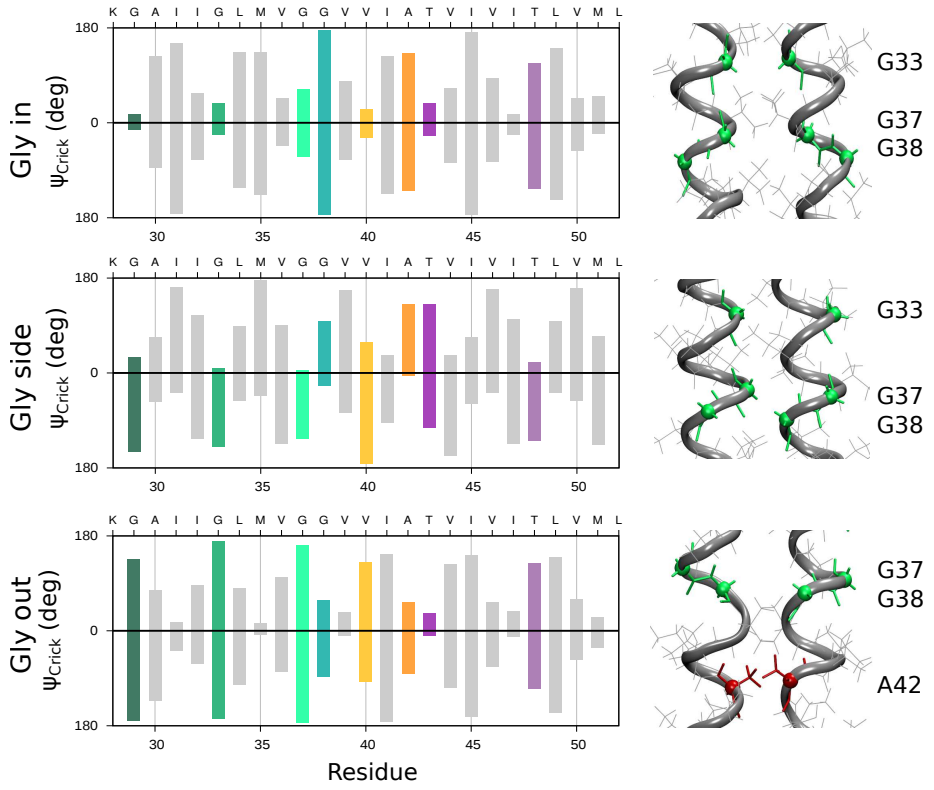

Figure 4.5: All-atom simulation results for the averaged ψ_{Crick} angles for conformations representing states Gly-in (top), Gly-out (center) and Gly-side (bottom), shown alongside characteristic structures derived from all-atom simulations in a POPC bilayer. Key glycine residues are shown in shades of green, residues V40 and A42 are shown in yellow and orange, respectively, and C-terminal threonine residues are shown in purple.

(1) "Gly-in" configurations (smallest d_{GG} in Fig. 4.4, upper) are characterized by close interpeptide contact facilitated by exposure of backbone carbonyls in the GxxxG repeat region. This structural motif is defined by "in phase" values of ψ_{Crick} (see Fig. 4.4, lower)

stabilized by contacts at an interface formed by G29, G33, and G37 (small values of ψ_{Crick} in Fig. 4.4), allowing V40 to remain near the interface while A42 faces outside (large value of ψ_{Crick} in Fig. 4.4). In addition, T43, I47, and a "lysine-zipper" stabilize interpeptide contacts in the C-terminal domain of the TM helix.

(2) "Gly-side" configurations (intermediate d_{GG} in Fig. 4.4) are characterized by substantial interhelical contact and interpeptide interactions involving hydrophobic residues Leu34 and Met35 that interact to form a zipper-like structure. This structural motif is defined by "out of phase" values of ψ_{Crick} (see Fig. 4.4). In this conformation, the I32, V36, V40, T43, and I47 side chain contacts form the interpeptide interface. These bulky hydrophobic side chains cause the backbones to be farther separated in a state that may serve as an "intermediate" in transitions between Gly-in and Gly-out states.

(3) "Gly-out" configurations (largest d_{GG} in Fig. 4.4) are characterized by glycine repeats facing the outside of the homodimer interface (large values of ψ_{Crick} in Fig. 4.4). In this conformation, I32, V35, and V39 side chain interactions stabilize an *X*-like homodimer structure (as was observed in recent NMR experiments). A larger interpeptide separation in the N-terminal region of the TM helix allows for close contact between G38 and A42/T43 that mediates the dimeric Gly-out interaction in the C-terminal region of the TM helix.

4.3.4 Membrane fluctuations influence the different states of $(\mathbf{C99}_{15-55})_2$

In order to better understand the effect of the environment on dimer structure, CG results were filtered based on local membrane fluctuations through the simulation. Separation of the CG dimer structures by their local hydrophobic core (defined by the 10Å hydrophobic section around the x and y center of geometry of the dimer), shows a direct correlation between the membrane width and the population of the different structural states. As shown in Fig. 4.6 (left), smaller hydrophobic cores increase the population of Gly-out conformations, while wider hydrophobic cores favor Gly-in conformations.

This trend was also seen in REMD simulations when simulations in the 42Å membrane

were compared to results from simulations run using narrower membrane parameters. In Fig. 4.6 (right), sampling in the smaller 40Å membrane shifts significantly to favor the Gly-side and Gly-out dimer states.

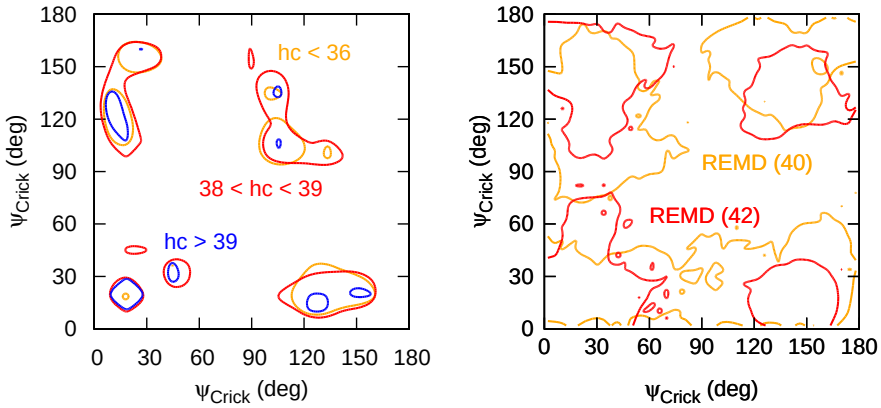

Figure 4.6: Left: Population of Crick angles in the CG simulation filtered by local membrane widths. Yellow clusters correspond to a local hydrophobic core (hc) smaller than 36Å, red to a local hc between 38 and 39Å, and blue to a local hc wider than 39Å. Right: Population of Crick angles from two separate REMD simulations; one in a 42Å membrane (red), and the other in a 40Å membrane (yellow).

Fig. 4.7 shows the fractional helicity by residue for the TM helix in each cluster in both all-atom and REMD simulations. Both CG and all-atom results suggest that the average helicity is similar in all states. In each case, there is a drop in helicity near the G37/G38 hinge, as well as a strongly helical nature that diminishes near V50, which is the site of initial cleavage by γ-secretase. These findings together suggest that changes in the dimer interface are not due to structural changes in the TM domain, but rather are an effect of the local membrane environment.

The three substates (Gly-in, Gly-side, and Gly-out) are characterized by distinct kink and tilt values (Fig. 4.8). The kink angles were calculated as the angle between the N-terminal and C-terminal portions of the TM helix (above and below residues G37/G38). The TM angle was calculated for the N-terminal portion of the TM helix, with the angle indicating the deviation from the membrane normal. In the Gly-in substate, both peptides

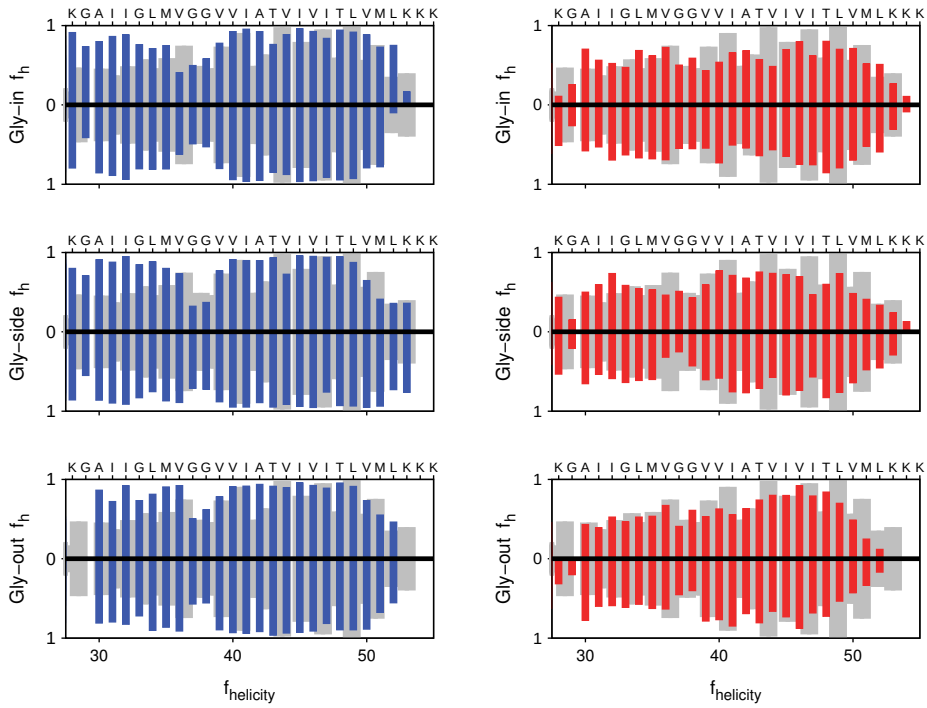

Figure 4.7: The helicity observed in the different all-atom simulation of $C99_{15-55}$ homodimer in a POPC bilayer (left) and REMD simulations in a GBSW membrane model (right). From top to bottom are Gly-in, Gly-side and Gly-out.

display a moderately kinked TM helix (kink angles up to ≈30-35 degrees) and one peptide is characterized by a larger tilt angle. The Gly-side structures are characterized by both peptides in the homodimer having relatively low kink and tilt angles, while the Gly-out substate is observed to contain both heavily tilted peptide, and one peptide having moderately larger kink values. These might indicate a possible mechanism for the effect of the bilayer environment on the dimer interface, where repositioning of the peptides to accommodate varying bilayer widths imposes steric effects as the homodimers interact with each other. Wider membranes would bias the peptides towards less tilted conformations, with the favorable right-handed GxxxG interactions requiring the peptide to coil around each other, yielding higher kink values. Intermediate membrane widths attenuate these interactions, decreasing the kink angles in the peptides. Narrow membrane widths require both peptides to tilt heavily to avoid hydrophobic mismatch of the peptides in the bilayer.

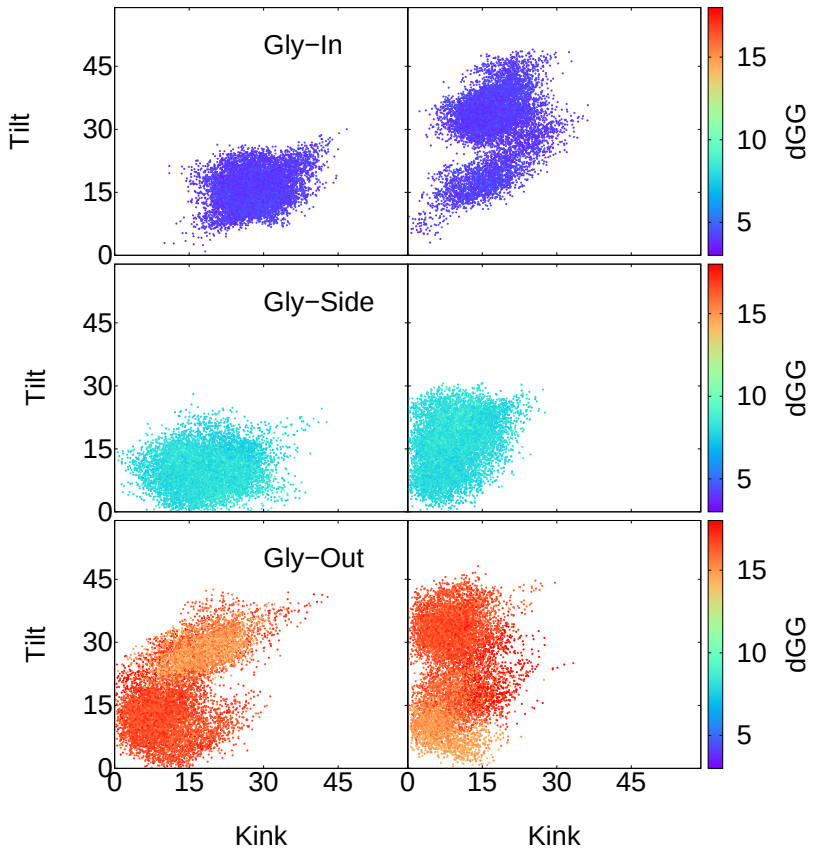

Figure 4.8: The kink and tilt angles observed in the different all-atom simulation of $C99_{15-55}$ homodimer in a POPC bilayer. Left and right sides show results for each peptide in the homodimer, respectively. From top to bottom are Gly-in, Gly-side and Gly-out. Color indicates the d_{GG} value in angstroms.

4.4 Discussion

It has been proposed that dimerization of the C99 transmembrane domain is a consequence of intermolecular interactions facilitated by GxxxG motif repeats [36]. This motif also promotes a right-handed crossing in JM helices by providing a good surface for packing and permitting close helix proximity [115]. The earliest proposed structures for the homodimer of the TM region of C99 were right-handed coiled-coil structures stabilized by favorable interactions at the interpeptide interface facilitated by the GxxxG motif. In contrast, two recently proposed NMR structures (PDB:2LOH [92], and 2LZ3 [116]) of the C99

TM sequence consist, respectively, of a left-handed and right-handed coiled-coil structure stabilized by interpeptide contacts facilitated by the G38xxxA42 repeat motif, which would correspond to a Gly-out orientation.

It is important to note that experimental studies of C99 were performed in a variety of lipid environments, including DMPC and DMPG membrane bilayers [98], LMPG micelles [67], DPC micelles and DMPC/DHPC bicelles [92], and neuronal cell systems [54] among others. It has been proposed in many of these studies that C99 is sensitive to the lipid environment, and that both its structure and cleavage can be affected by changes in the environment [36, 67, 90].

In this study, we find that $C99_{15-55}$ homodimers consist of an ensemble of structures, stabilized by varying interfaces, including both GxxxG and GxxxA motifs that have been previously characterized experimentally. Although the dimers favor a right-handed coiled-coil packing, left-handed structures exist within the ensemble as well. Furthermore, we find that the sampling of these states is strongly correlated to the local membrane fluctuations, with narrower bilayers yielding a Gly-out orientation stabilized by the more C-terminal GxxxA motif, and slightly wider membranes adopting the originally proposed Gly-in structure characterized by close packing of the N-terminal GxxxG repeats.

We believe that the strong sensitivity of the dimer structures to changes in the local hydrophobic environment - on the order of a few angstroms - yields insight as to why experimental studies performed in a variety of micelle and bilayer systems of differing lipid compositions result in such contrasting dimer structures that involve different residues at the interface and expose different residues at the homodimer surface. This suggests a possible mechanism for how varying lipid composition, as well as the presence of cholesterol might affect local membrane character, and thus the structure and processing of C99 dimers [67, 90]. Our work suggests a possible mechanism for "environmental-selection" of specific C99 homodimer substates, even before consideration of possible specific peptide-cholesterol interactions.

Chapter 5

Impact of membrane lipid composition on the structure and stability of homodimers of the transmembrane domain of Amyloid Precursor Protein [1]

5.1 Introduction

Understanding the structural and thermodynamic properties of transmembrane helical dimers is of fundamental importance to molecular biology. It is known that the association of "biotopic" proteins, having single transmembrane (TM) helical domains, is essential to immunoreceptors and protein kinases that play critical roles in cellular function. Insights from computation and experiment have since led to an appreciation for the role of sequence-specific interactions stabilizing helix dimerization [117]. Of particular interest is the role of the GxxxG motif in stabilizing TM helix-helix association in systems including the glycophorin A (GpA) homodimer [56, 118], found in the human erythrocyte membrane, and APP-C99 (C99), the 99 amino acid C-terminal fragment of the amyloid precursor protein [98, 100].

The amyloid β (Aβ) peptide aggregation pathway, known to be critical to the evolution of Alzheimer's Disease, begins with the cleavage of APP-C99, by γ-secretase leading to formation of Aβ. The formation of homodimers of APP-C99 has been proposed to be critical to the processing by γ-secretase, a process that is known to depend on a number of factors including peptide sequence and lipid composition of the membrane environment. Knowledge of the structure and stability of the APP-C99 (C99) homodimer is therefore critical to our understanding of the Aβ peptide aggregation pathway.

The first simulation of an equilibrium structural ensemble of the homodimer of the

[1] All coarse-grained and all-atom simulations and analysis in this chapter were performed by Dr. Laura Dominguez.

TM helical region of C99, $C99_{23-55}$, was performed using replica exchange molecular dynamics (REMD) simulation and an implicit membrane model [100]. The structure of the WT homodimer was found to be a λ-like right-handed coiled-coil structure stabilized by interpeptide C_α hydrogen bonds, mediated by interactions between GxxxG motifs. Of the three contiguous GxxxG motifs in the WT peptides the C_α hydrogen bonds involving Gly_{33} and Gly_{38} were observed to be most essential in stabilizing the WT dimer. The simulated structural ensemble was in good agreement with the proposed solid state NMR structure [98] while providing more detailed insight into the structural ensemble of the dimer in a fluid membrane environment.

Additional support for this structural motif for the homodimer was provided in a recent study involving H/D exchange experiments on the C99 peptide complemented with molecular dynamics simulations of the TM region, $C99_{28-55}$, in a POPC bilayer. That study also provided detailed insight into the stability of helical regions of C99 including the TM helix. It was found that the portion of the TM helix on the N-terminal side of the G37/G38 "kink" was more dynamic and showed enhanced H/D exchange relative to the C-terminal portion of the TM helix [29]. That finding is in agreement with prior studies of the C99 monomer in LMPG micelles. It is also in agreement with prior simulation studies [100] of the WT $C99_{23-55}$ homodimer demonstrating that the region of the peptide including the GxxxG repeats was significantly less helical than the C-terminal portion of the TM helix, allowing for close interpeptide backbone association and C_α hydrogen bonding stabilizing the homodimer [100].

In addition, a recent NMR study led to the first experimentally derived structure of the homodimer formed by the TM helical domain, $C99_{23-55}$[92]. In contrast to earlier computational modeling and simulation predictions, the proposed structure is a X-like left-handed parallel dimer stabilized through interactions involving an extended heptad repeat motif TM helical region. This study raises additional questions related to the peptide environment, focusing on how factors such as micelle size and interfacial curvature might

influence peptide structure[119, 120, 121].

Importantly, an NMR study of $C99_{1-55}$ in membrane environments of variable lipid composition clearly demonstrated that fluctuations in the TM helix can be a strong function of membrane composition [36]. Changes in membrane composition may modulate the physical boundaries of the bilayer, including width and structure of the interface, as well as the chemical nature of the head group region and membrane interior. While it is clear that C99 peptide structure depends on membrane compositions, the role of these various physical-chemical parameters in influencing the peptide structure is not understood.

To explore these important open questions, we have performed a detailed simulation study of the structure and stability of the homodimer of the TM domain of APP-C99 using a multiscale computational model. This approach aspires to use atomistic and coarse-grained representations of the peptide and lipid system self-consistently, in a manner that allows for the study of the homodimer structure and its dependence on membrane composition. Our results provide a detailed picture of the $C99_{23-55}$ structural ensemble, its dependence on membrane composition, and the potential role for changes in structure to influence function of this critical amyloid precursor protein.

5.2 Methods

A multiscale computational approach was employed, as described in Chapter 2 combining implicit replica exchange MD (REMD) simulations [57], coarse-grained models of the protein, lipids, and solvent using the Martini force field [59, 60], and all-atom representations of the protein using all-atom CHARMM and GROMOS force field models for the protein, membrane, and solvent environments [61, 62, 63, 64].

Initial conditions for the homodimer simulations were taken from experimentally derived structures determined by NMR of $C99_{(15-55)}$ in zwitterionic dodecylphosphocholine (DPC) micelles (PDB 2LLM) [92]. Additional initial conditions were taken from experimentally derived monomeric structures determined by NMR of $C99_{(1-55)}$ in lyso-myristoylphosphatidylglycerol

(LMPG) micelles (PDB 2LMT) [67, 90]. The initial structures for the coarse-grained simulations of monomers and dimers were generated using a mapping from the NMR and REMD simulations. The structures were embedded in pre-equilibrated coarse-grained lipid bilayers of varying composition, including pure DMPC, pure DPPC, pure POPC, and POPC/DOPE 1:1 (mol:mol) mixture.

Table 5.1: System sizes and time scales for implicit solvent, coarse-grained, and all-atom simulations.

System	Time	Bilayer	Force field
$2 \times C99_{23-55}$	10 ns	Imp 27 Å	REMD CHARMM27
$2 \times C99_{23-55}$	10 ns	Imp 30 Å	REMD CHARMM27
$2 \times C99_{23-55}$	10 ns	Imp 32 Å	REMD CHARMM27
$2 \times C99_{23-55}$	10 ns	Imp 35 Å	REMD CHARMM27
$2 \times C99_{23-55}$	10×1.5 μ s	DMPC	MARTINI2.2
$2 \times C99_{23-55}$	10×1.5 μ s	DPPC	MARTINI2.1
$2 \times C99_{23-55}$	10×1.5 μ s	POPC	MARTINI2.1
$2 \times C99_{23-55}$	10×1.5 μ s	POPC/DOPE	MARTINI2.1
$C99_{23-55}$dim(A)	100 ns	POPC	CHARMM36
$C99_{23-55}$dim(B)	100 ns	POPC	CHARMM36

The replica-exchange molecular dynamics (REMD) simulations were performed using the CHARMM22 force field [122], with an all-atom model of the protein combined with an implicit representation of the solvent and membrane environments using the GBSW model [58]. In the coarse-grained simulations, non-bonded interactions were calculated within a cutoff of 1.2 nm using shift functions (between 0.9 and 1.2 nm for Lennard-Jones interactions and between 0 and 1.2 for electrostatics) [59]. The temperature of the systems was set to 325 K using the Berendsen weak coupling method [106] with a coupling time of 0.1 ps. The pressure was set to 1 bar using a semi-isotropic coupling scheme with lateral and perpendicular pressures coupled separately with coupling time 0.1 ps and compressibility of $2{\times}10^{-5}$ bar^{-1} [106]. An integration time step of 30 fs was used in all simulations. For the all-atom simulations, the short range electrostatics was cut-off at 1.2 nm. PME was used to calculate the long-range electrostatics interactions. To control the temperature and pressure, the Nosé-Hoover (16) thermostat and the Parrinello-Rahman barostat were employed. Simulations details for all systems are shown in Table 5.1.

5.3 Results

Conformational distributions were derived from both replica-exchange molecular dynamics (REMD) or coarse-grained (CG) molecular dynamics simulations. REMD simulations consisted of 16 replicas spanning temperatures from 300-550K with 10 ns of simulation for each replica (160 ns total simulation time) for each system. $C99_{23-55}$ homodimer systems were simulated in four different GBSW implicit membrane widths: 27, 30, 32, and 35 Å, respectively. Starting configurations sampled a variety of dimer interfaces, with the peptides placed 25 Å apart. CG simulations were performed using 10 replicas with 1.5 μs of dynamics for the $C99_{23-55}$ homodimer in DMPC, DPPC, POPC, and 50:50 POPC/DOPE bilayers. The two monomers were initially placed at a separation of 50 Å and allowed to associate.

5.3.1 Conformational ensemble of $C99_{23-55}$ homodimer consists of multiple conformational substates

Important order parameters used to characterize the homodimer ensemble include the dihedral angle formed by G_{29}-G_{37}-G_{37}-G_{29} (ϕ_{4G}), which differentiates right-handed (negative values) and left-handed (positive values) coiled-coil geometries, and d_{GG} distance, where close distances indicate interpeptide contacts in the GxxxG repeat region. Simulations of the homodimer were analyzed using a projection of the homodimer ensemble on the the ϕ_{4G} angle and the d_{GG} distance between the homodimers in bilayers of varying lipid composition (Fig. 5.1).

We identify three populated substates that contribute to the homodimer ensemble. The conformations within each substate are uniquely identified in terms of one of three different packing interfaces. (1) The most populated configuration ("Gly-in") is stabilized by Gly-Gly interactions in which the residues of the ϕ_{4G} repeat face the inside of the homodimer structure with d_{GG} distances of 5 Å and ϕ_{4G} angles of <-25 degrees. (2) The next most populated ("Gly-side") substate is defined by stabilizing interpeptide interactions involving

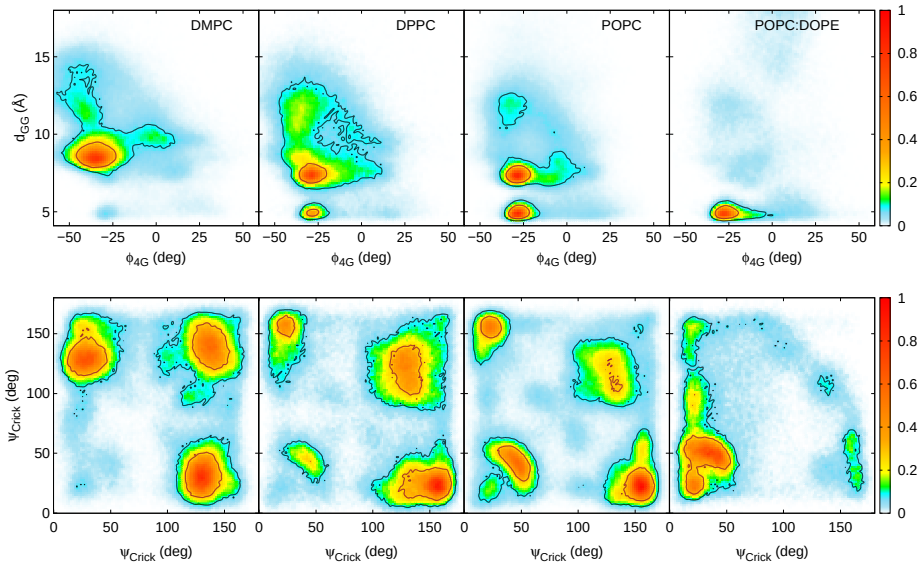

Figure 5.1: Conformational distributions derived from CG MD simulations. While the overall conformational ensemble is dominated by right-handed coiled-coil conformations for each bilayer, the lipid composition is observed to modulate the relative stability of competing substates in the homodimer structural ensemble. Colors indicate relative population distributions.

the hydrophobic residues Leu34 and Met35 that interact to form a zipper-like structure (with glycine facing the side of the homodimer interface). (3) The least populated ("Gly-out") substate is characterized by having the glycine repeats facing the outside of the homodimer interface leading to stabilization of the homodimer by hydrophobic interpeptide interactions with d_{GG} distances of 12 Å.

Fig. 5.1 and Fig. 5.2 display the probability distributions for the ϕ_{4G} angle and d_{GG} distance for the $C99_{23-55}$ homodimer in four different CG and implicit membrane systems, respectively. While right-handed homodimers are dominant in all membrane compositions, there are notable changes in the relative probability of the three conformational substates that compose the homodimer's conformational ensemble. In particular, in moving from the shortest to longest alkyl chains in saturated DMPC, saturated DPPC, and monounsaturated POPC, and finally to the mixture of POPC and diunsaturated DOPE, there is a dramatic

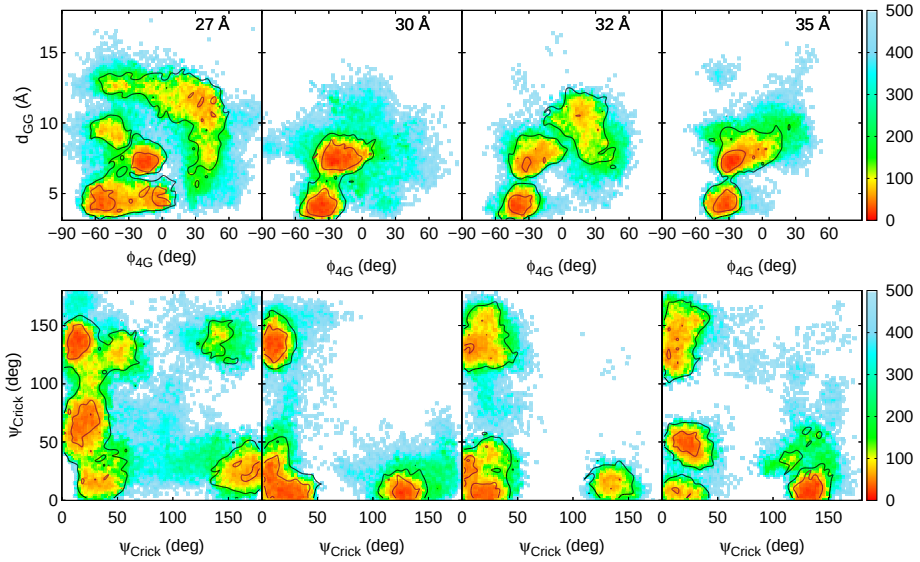

Figure 5.2: Conformational distributions derived from REMD simulations. The simulations favor right-handed structures at lower d_{GG} values, although structures with larger d_{GG} values also sample left-handed structures. The relative sampling of each substate shifts as the width changes, with the 32 Å membrane homodimer structural ensemble strongly dominated by the Gly-in state. Colors indicate Free Energy in kcal/mol.

shift in populations of the three homodimer substates. This same shift is reflected in the implicit membrane systems as the GBSW membrane width is increased.

5.3.2 Membrane lipid composition modulates competing $C99_{23-55}$ homodimer substates

The shift in substate populations can be understood in terms of the lipid density profiles for the four bilayers (see Fig. 5.3). In the thinnest membrane systems, DMPC (CG) / 27 Å (GBSW), the homodimer has the broadest distributions of ϕ_{4G} angle, and the most substantial populations in the "Gly-out" substate. As the lipid composition is varied and the membrane width increased, there is a transition to an increasingly sharply defined value of ϕ_{4G} angle and enhanced population of the "Gly-in" substate. For the thickest membrane,

POPC/DOPE, there is a strong preference of the "Gly-in" substate that is consistent with the earliest predictions of the $C99_{23-55}$ homodimer structure. However, we see that the particular homodimer structure, and the intrinsic disorder in the conformational ensemble, is a strong function of membrane composition.

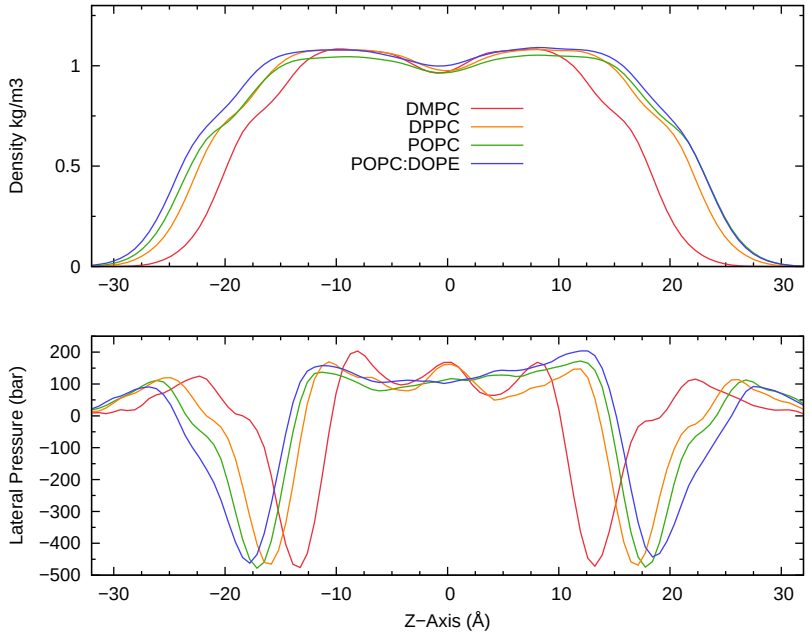

Figure 5.3: Lipid density profiles derived from CG MD simulations in four bilayer lipid compositions (from the top) DMPC, DPPC, POPC, and 50:50 POPC/DOPE.

In clear support of this observation, the tilt angle distribution (see Fig. 5.4) shows a dramatic increase of ≈20 degrees for states sampled by homodimers in the 27 and 30 Å implicit membrane as opposed to the 35 Å system (where the tilt angle samples a narrow distribution centered around 20 degrees).

5.3.3 Homodimer substate population is a sensitive function of membrane width

Although the homodimer systems in Fig. 5.2 sample many similar ϕ_{4G} and d_{GG} values, systems in varying membranes do not necessarily adopt the same structures. Fig. 5.5

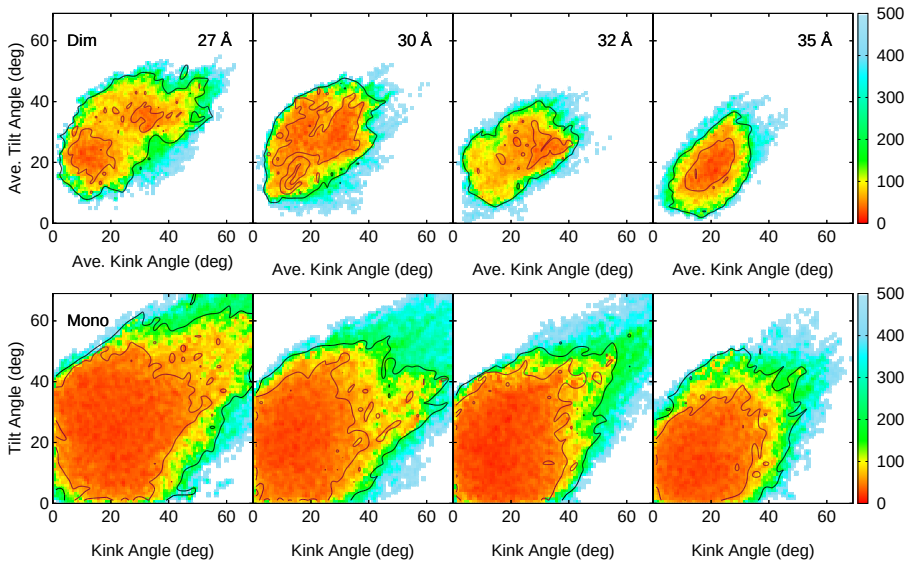

Figure 5.4: Peptide kink and tilt angle distributions derived from REMD simulations. Top: $C99_{23-55}$ homodimer systems, with angles are averaged over both peptides. Bottom: $C99_{23-55}$ monomer. Colors indicate Free Energy in kcal/mol.

presents values for the same order parameters for the lowest energy replica in each implicit membrane system now colored by the maximum peptide kink angle in the homodimer. The average peptide kink varies substantially with the membrane width parameter (Fig. 5.4). Comparing the distributions for the 27 Å and 35 Å membranes in Fig. 5.5 one can see clear differences between clusters with similar d_{GG}/ϕ_{4G} value. Structures in the 27 Å membrane display significantly higher maximum kink angles, nearly 90 degrees, whereas the same cluster in the 35 Å membrane has a maximum kink angle around 30 degrees.

5.3.4 Helicity of $C99_{23-55}$TM helix is enhanced by homodimer formation

In order to develop a detailed atomistic description of the protein-protein interactions of the most probable CG homodimeric structures, we performed all-atom molecular dynamics simulation using the CHARMM force field in a variety of lipid membranes and analyzed the resulting structural distributions. Initial structures were chosen from the result of CG

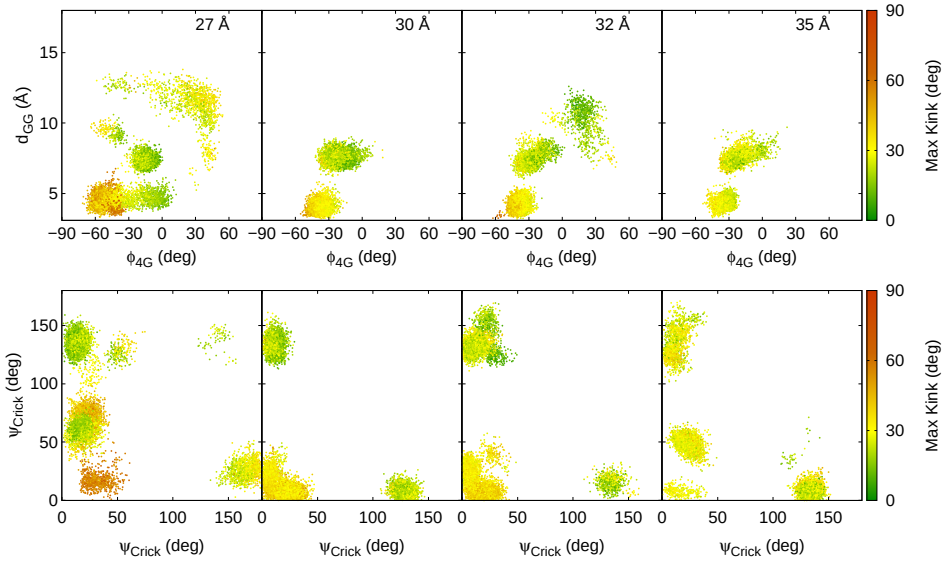

Figure 5.5: Distributions derived from REMD simulation of $C99_{23-55}$ homodimer systems in varying implicit GBSW membranes. Results derived from the lowest energy replica of each system are plotted by (top) ϕ_{4G} and d_{GG} values and (bottom) ψ_{Crick} angles. Color indicates the value of the maximum kink angle in the homodimer.

MD simulations representing the "Gly-in" and "Gly-out" substates in a POPC membrane. Using Pulchra [104] we transformed the initial coarse-grained structures to all-atom models, which were embedded in a POPC membrane using CHARMM/GUI. The structures were minimized and pre-equilibrated at 303 K and 1 atm while restraining the protein backbone, followed by a production run in the absence of restraints under a NPT semiisotropic ensemble using CHARMM36 all-atom lipid force field (with CMAP) and TIP3P water.

Our all-atom simulations confirm that the secondary structure of $C99_{23-55}$ is predominantly helical as a monomer and as a homodimer (Fig. 5.6). The root-mean-square fluctuation in the TM helix of the monomeric peptide is consistent with experimental data presenting the largest motion near Gly 39 [90]. We detect an enhancement in the helicity of the TM region in the homodimer relative to the monomer. It appears that fluctuations in the monomeric peptide, particularly near the proposed "kink" region of the TM helix,

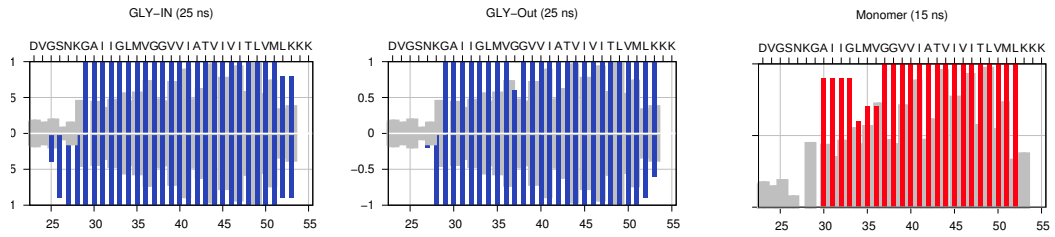

Figure 5.6: The average helicity derived from all-atom simulation of $C99_{23-55}$ monomer (red) and homodimer (blue) in a POPC bilayer using an all-atom model. The grey shadow shows experimentally determined helicity based on NMR chemical shift measurements for monomeric $C99_{1-55}$ in an LMPG micelle [67].

reduce helicity in the monomer while being somewhat suppressed by interpeptide contacts in the homodimer.

5.3.5 Other transmembrane helix-helix interactions

Among other transmembrane proteins, glycophorin A (GpA) dimerization has also been proposed to be a consequence of interactions facilitated by GxxxG motif repeats forming right handed coiled-coils [118, 117, 65]. However a diversity of structures of coiled-coils interactions have been found in TM helices: homo- or hetero-dimers with right or left-handed crossing angle between the helices and dynamic conformations of TM helix dimers have been proposed to be essential for physiological function of TM proteins [123, 124, 125]. An interesting coiled-coil TM helix is the human EphA2 receptor tyrosine kinase because it has been proposed that its dimeric conformation is affected by the thicknesses of the lipid bilayer; in thick bilayers EphA2 TM forms a left-handed (+15) TM dimer stabilized via an heptad repeat motif while in thiner membranes the EphA2 TM dimer is characterized by a glycine zipper motif and a right handed (-45) crossing angle between the helices.

We carried out CG simulations of EphA2 homodimer in bilayers of varying lipid composition (see. Fig. 5.7) to compare with trends observed in our simulations of the $C99_{23-55}$ homodimer. We observe structures consistent with both the "Gly-in" and "Gly-out" sub-

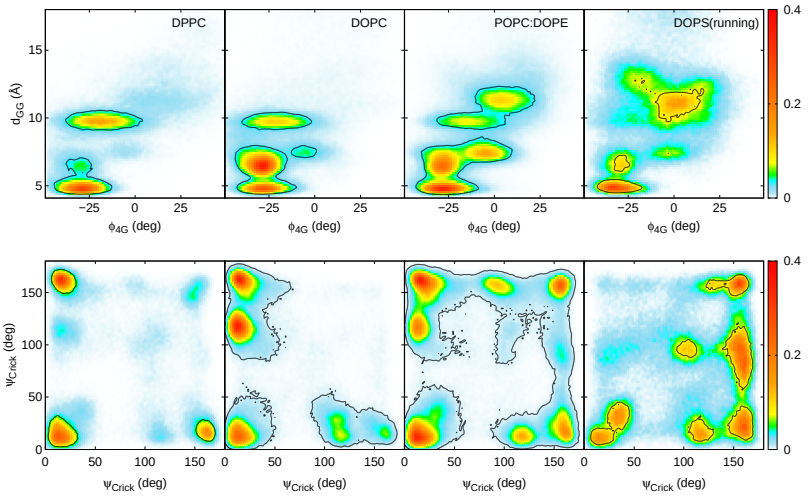

Figure 5.7: Conformational distributions derived from CG simulation of EphA2 homodimer systems in bilayers of varying lipid composition, plotted by (top) ϕ_{4G} and d_{GG} values and (bottom) ψ_{Crick} angles. Color indicates relative probability. Substantial dependence of the homodimer structure, including variations in handedness of the coiled-coil, on bilayer lipid composition is observed.

states, with an overall ensemble that is dominated by right-handed coiled-coil structures. Moreover, the same substates forming this structural ensemble are observed in four different membrane environments. These results based on a multiscale modeling approach that accounts for a detailed picture of the protein-lipid interactions provides clear support for the dominance of the right-handed coiled-coil structure for the WT $C99_{23-55}$ homodimer in a lipid bilayer. The simulations further suggest that lipid composition may be critical in determining the degree of helicity in the transmembrane region, which appears to be enhanced in the homodimer relative to the monomeric peptide.

5.4 Discussion

Lipid composition of membranes has been shown to impact the structure and stability of C99 homodimers as well as the integrity of the TM helical region in the monomeric peptide. Our multiscale simulations have explored the structure of the $C99_{23-55}$ monomer and homodimer in bilayer membranes as a function of varying lipid composition. Overall,

our results suggest that a multiscale approach to modeling TM helical association in lipid bilayers, critical to biomolecular signaling and processing, can provide critical insight into the relationship between protein structure and function.

Our results support earlier simulation predictions, based on simplified models or limited experimental information, that the homodimer structure of $C99_{23-55}$ is a right-handed λ-like coiled-coil stabilized by interpeptide interactions. However, we also find that the particular lipid composition of the membrane impacts the bilayer width which biases the TM helix tilt orientation of the monomeric $C99_{23-55}$ structure in the membrane. Our simulations identify three conformational substates that define the overall right-handed coiled-coil homodimer ensemble. The particular importance of one substate relative to another is modulated by the lipid composition of the membrane bilayer. Results for $C99_{23-55}$ homodimer structure derived from REMD simulations in implicit membrane of varying thickness are in qualitative agreement with trends observed CG simulations of $C99_{23-55}$ homodimer in explicit bilayers of varying lipid composition (see Figs. 5.2 and 5.7).

The trends observed in the structural ensemble of the $C99_{23-55}$ homodimer as a function of lipid membrane composition also provides a partial explanation for the recently observed NMR structure of the $C99_{15-55}$ homodimer in a DPC micelle [92]. That structure was observed to have a "Gly-out" structure that differed from the previously proposed "Gly-in" structures that were based on simulation and solid-state NMR data [54, 51, 98, 100, 91]. The surfactant forming the DPC micelle is most similar in structure and alkyl chain length to the DMPC lipid, which was found to form the thinnest of the four lipid bilayers studied. In that thin membrane, the tilt angle was enhanced and the "Gly-out" structure significantly enhanced over the structural ensembles observed in the thicker bilayers. Therefore, the "Gly-out" configuration observed experimentally may, at least in part, reflect the relative restraints of the "thin" micelle in which the $C99_{23-55}$ homodimer was studied.

It has been observed that membrane thickness is a crucial factor in the processing of APP by γ-secretase that can impact the overall production of Aβ peptide and the ratio of

Aβ_{40} : $A\beta_{42}$. Our results demonstrate that membrane composition can influence membrane thickness, which can both alter the depth of insertion of the peptide into the membrane and impact the termination of processive cleavage of the TM helix by γ-secretase. Moreover, our results demonstrate that membrane lipid composition can impact the structure and stability of the C99 homodimer, with thicker membranes stabilizing "Gly-in" conformations, another factor that has been shown to impact the processing of C99 by γ-secretase.

Chapter 6

Flemish A21G familial Alzheimer's Disease mutation alters APP-C99 homodimer interface

6.1 Introduction

According to the Amyloid Cascade Hypothesis, accumulation of amyloid β (Aβ) is the crucial event leading to the development of Alzheimer's Disease (AD) [8, 81]. A key step in the "cascade" is the processing of Amyloid Precursor Protein (APP) to generate the Aβ peptide. APP is a type I transmembrane protein of lengths ranging from 365 residues to the more common 770 residues [14, 7]. In the amyloidogenic pathway, APP is initially processed at the N-terminus of Aβ by β-secretase [15, 17], releasing a large extracellular domain and leaving behind a membrane-bound 99-residue long fragment. This fragment, known as C99, undergoes multiple sequential cleavage events by the protein complex γ-secretase, beginning at the ϵ-processing and progressing up the TM helix to the final γ site, which releases the resulting Aβ protein [22, 24, 25].

Two main pathways have been identified for this cleavage mechanism: one beginning with ϵ-cleavage at residue L49 and progressing to Aβ40 cleavage, the other with the ϵ-site shifted to residue T48, generating Aβ42 [29]. What influences the favorability of one pathway over the other remains an open question, however many known Familial Alzheimer's Disease mutations (FAD) have been shown to alter the ratio of Aβ42/Aβ40, leading to early onset of AD [85, 87].

In 1992, researchers identified a new FAD mutation, coded by a C$\rightarrow$G base pair mutation at exon 17 [44]. This mutation was associated with an early onset of AD ($\approx$46 years of age), and was accompanied by cerebral haemorrhage and early age of death. This Flemish mutation - A21G substitution on the C99 protein - has been suggested to operate by a

different mechanism than many other characterized FAD mutations. The A21G mutation has been demonstrated to increase production of both Aβ40 and Aβ42 by amounts ranging from a two- to four-fold increase [45, 126, 91]. Proposed theories include that A21G mutation creates a better substrate for γ-processing, or that the central hydrophobic cluster (CHC) on the Aβ strand (residues $\mathrm{L}^{17}VFFA^{21}$) acts as a γ-secretase inhibiting region and that mutation at residue 21 reduces inhibition [126, 91].

The A21G mutation has also been investigated for its effect on APP dimerization [91]. The APP strand contains GxxxG repeat motifs which have been shown though both simulation and experiment to enhance dimerization by enabling close interpeptide contacts [54, 53, 29, 100, 121]. The WT sequence features three sequential repeats of this motif: G25xxxG29xxxG33xxxG37. The A21G mutation extends this motif by one repeat, and adds the G21xxxG25 sequence, and a recent study suggested that the A21G mutation might be responsible for a change in the dimer interface along the GxxxG repeats [91].

To investigate the effect of A21G substitution on the structure of APP-C99 homodimers, we carried out simulations of $\mathrm{C99}_{15-55}$ systems: WT and A21G mutants using a multiscale approach. Homodimers were simulated both in an implicit environment using the replica exchange (RE) method and in POPC bilayer. We hope to provide a better understanding of the effect of the A21G mutation to the structure and dimerization of C99, in order to characterize effects on the C99 system itself as opposed to possible effects on direct interactions with γ-secretase caused by the amino acid substitution.

6.2 Methods

6.2.1 Multiscale Simulation

As described in Chapter 2, this study employed a "multiscale" approach consisting of replica-exchange molecular dynamics (REMD) [57] simulations in a GBSW implicit membrane environment [58], as well as all-atom simulation in a POPC bilayer. The combination of

these methods allows for detailed investigation of the role of sequence in peptide structural ensembles. First, comprehensive sampling is obtained using the REMD method, where noninteracting replicas are simulated across a range of temperatures and allowed to attempt exchanges between neighbors at certain time steps according to the Metropolis criterion [57]. Assuming adequate overlap between energy distributions at adjacent temperatures, replicas are free to diffuse across the temperature space, allowing them to escape local minima and perform adequate sampling of the conformational space of the peptides.

Characteristic structures from the REMD simulations are then used to seed all-atom simulation in explicit lipid and water environments. This allows for detailed investigations of specific structural features, as well as water-peptide and lipid-peptide interactions which are lost in the implicit GBSW model.

6.2.2 Initial homodimer structure

Each peptide in the WT $C99_{15-55}$ peptide homodimers consisted of the sequence:

$$Q^{15}KLVFF^{20}\mathbf{A}EDVG^{25}SNKGA^{30}\ IIGLM^{35}VGGVV^{40}IATVI^{45}VITLV^{50}MLKKK^{55}$$

Starting structures for each peptide were taken from experimentally reported structures derived with NMR studies of $C99_{15-55}$ in DPC micelles (PDB 2LLM without N-terminal caps) [67]. The homodimers were constructed by taking the separate peptide chains and rotating them to sample a variety of initial interfaces between the peptides. Each generated homodimer structure was minimized and oriented along the membrane normal. In addition to the wild-type peptide, the A21G mutant was investigated, where the alanine at residue 21 (shown in bold) was replaced by a glycine residue. The point mutation was constructed in VMD [68], and the resulting homodimers were minimized in CHARMM before equilibration and production runs.

6.2.3 Simulation Parameters and Force Fields

REMD simulations were carried out using the MMTSB tool set [72]. 24 replicas were used, spanning a temperature range of 300 to 650 K. The MD timestep was set to 2 fs, with the timestep for neighboring replicas to attempt exchanges set to every 0.5 ps. The total simulation time for the WT system was 252 ns (10.5 ns/replica), and total simulation time for the A21G system was 192 ns (8 ns/replica). The last half of the simulations were used for analysis for both systems to avoid any dependence on initial conditions.

REMD simulations were performed in CHARMM [69] using an all-atom model of the protein, and implicit representation of the solvent and membrane environments using the Generalized Born model with a switching function (GBSW) [58]. The proteins were modeled using the CHARMM PARAM22 force field with dihedral cross-term corrections (CMAP) [70], and with corrected atomic radii for the GBSW model [71]. At the dielectric boundaries, a smoothing length of 0.6 Å was used, with 24 radial integration points, and a cutoff of 20 Å. The surface tension coefficient was set to 0.04 kcal/(mol $\cdot$ Å^2). The membrane was set to a total width of 42 Å, with 10 Å at each end defined as the "head group" switching region. This left a total of 22 Å as the membrane interior, where the dielectric value was set to 1. The switching function for the head group region then varied from the interior value to the solvent region, with a dielectric value of 80. The membrane was defined as a continuous slab in the xy-plane, with the membrane normal along the z-axis.

Representative frames were selected from clustering analysis of the REMD results and used as "seed structures" for all-atom simulations performed in GROMACS [76, 77] using the CHARMM36 protein and lipid force field, and the TIP3P water force field [78, 79]. Homodimer structures were embedded into pre-equilibrated POPC bilayers consisting of 128 lipid molecules (64 each on the top and bottom layers), completed with the addition of TIP3P water molecules extending 20 Å on each side of the bilayer, and six chloride counterions to establish electroneutrality. The full systems were constructed using the CHARMM-GUI [73, 74, 75]. All structures were subjected to steepest descent minimization,

followed by 100 ps of NVT and 2 ns of NPT equilibration before being simulated for 100 ns, with the initial 50 ns excluded from analysis. All equilibration and simulation used a time step of 2 fs, PME to calculate long-range electrostatics, with short-range electrostatics cut off at 1.0 nm. A Nosé-Hoover thermostat was used along with a Parrinello-Rahman barostat to control the temperature and pressure [80].

6.3 Results

6.3.1 A21 mutation alters homodimer peptide-peptide interactions

In order to adequately sample the configurational ensemble of the peptides, REMD simulations in an implicit GBSW membrane [58] were performed for both the wild-type (WT) and A21G mutant $C99_{15-55}$ systems. While specific lipid-protein interactions are lost in the implicit membrane model, the REMD method allows for comprehensive sampling of peptide-peptide interactions within the homodimer system [57] in order to provide a variety of starting structures for all-atom simulation.

In order to characterize the dimer interface, two main approaches were used: (1) projection onto the d_{GG} and ϕ_{4G} order parameters, and (2) the ψ_{Crick} angles for the homodimers. The distance (d_{GG}) is calculated between residues G33 on each peptide in the homodimer, and the ϕ_{4G} angle is given as the dihedral angle between residues $G33_A$-$G37_A$-$G37_B$-$G33_B$ where A and B indicate the respective peptides. Negative ϕ_{4G} values indicate right-handed coiled-coil interactions, while positive values indicated left-handed interactions.

Mutation at residue A21 has a clear effect on the peptide-peptide interactions involved in the dimer interface (Fig. 6.1). Whereas the WT system features dominant right-handed Gly-in interactions (small d_{GG} values), the A21G ensemble samples more broadly from a variety of substates, including both left- and right-handed interactions at a range of d_{GG} values.

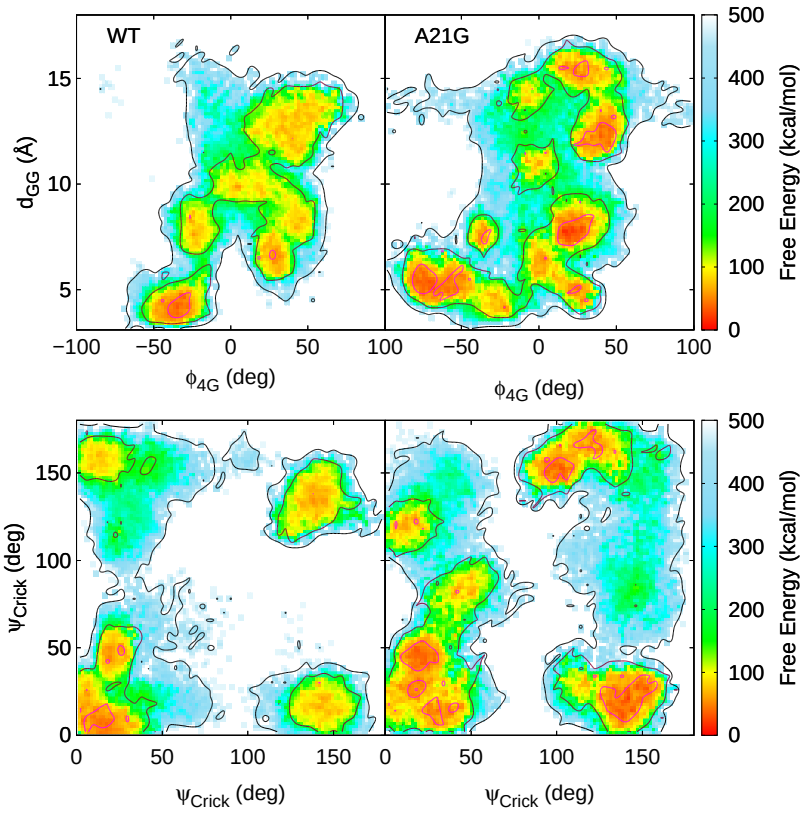

Figure 6.1: Conformational distributions of $C99_{15-55}$ in implicit membrane derived from REMD simulations for the WT (left) and A21G (right) $C99_{15-55}$ sequences, projected onto key order parameters: (top) d_{GG} and ϕ_{4G} values and (bottom) ψ_{Crick} angles.

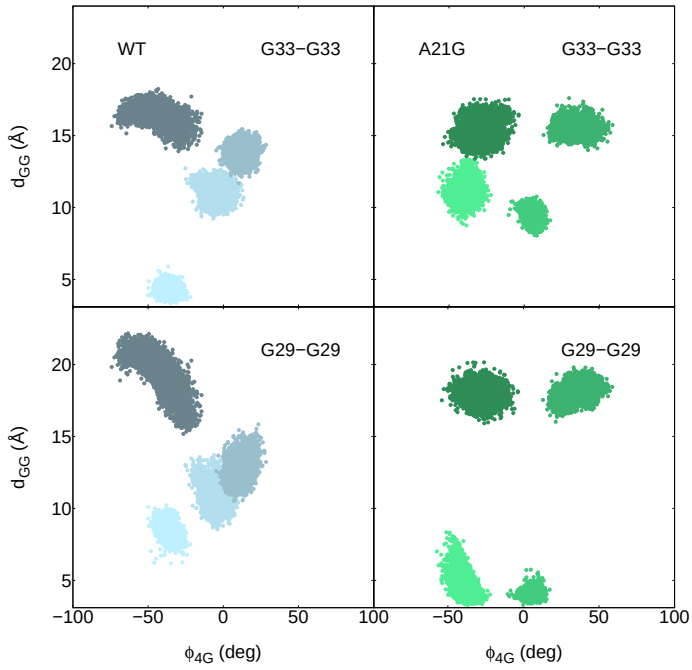

Figure 6.2: Distributions of $C99_{15-55}$ peptides in POPC bilayer derived from all-atom simulations, showing projection of each simulation onto the d_{GG} and ϕ_{4G} order parameters for the WT system (left, blue) and A21G system (right, green). The d_{GG} value was calculated as the distance between residues G33 (top) as well as between G29 (bottom). Relative shade of points indicates a specific all-atom simulation.

6.3.2 A21G mutation alters GxxxG motif interactions

From the REMD simulations, representative frames were selected from both the WT and A21G mutant systems to seed all-atom simulations. In order to simulate a variety of structures, four frames were selected from both systems: left- and right-handed coiled-coil structures at both small and large d_{GG} values. In the WT system, the RH Gly-out frame was taken from a simulation performed in a narrower, 30Å implicit GBSW membrane, in which that region was more heavily sampled. These characteristic homodimer structures were embedded in a POPC bilayer for 100 ns of simulation time.

As we have shown in previous studies [121], the WT $C99_{15-55}$ homodimer system is best characterized by interactions between residues G33 on each strand. Along the repeating

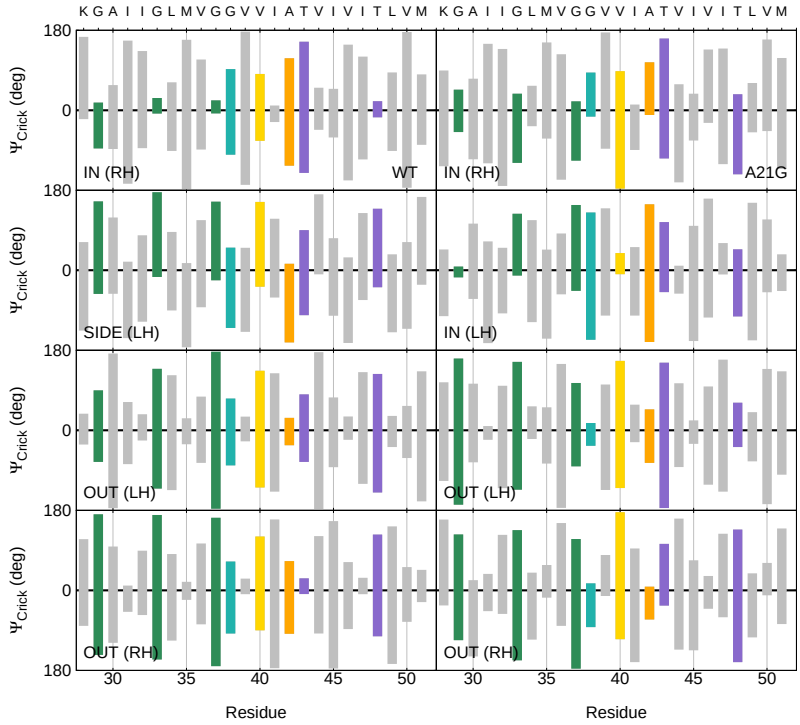

Figure 6.3: Average ψ_{Crick} angles for each residue derived from all-atom simulations of $C99_{15-55}$ homodimers in POPC bilayer for all structures in the WT system (left) and A21G system (right). Important residues are highlighted: glycine repeats (dark green), G38 kink location (teal), V40 (yellow), A42 (orange), C-terminal threonines (purple). Shades indicate respective peptides in the homodimer.

GxxxG motif, the G33 residues are responsible for close interactions stabilizing the Gly-in structure. This is seen in Fig. 6.2 (upper left) by the right-handed Gly-in cluster. Other characteristic clusters for the WT system included: a Gly-side cluster (intermediate d_{GG} values, predominantly left-handed), and two separate left- and right-handed Gly-out clusters (large d_{GG} values). In the A21G system, however, projection onto the G33 d_{GG} values yielded no close interactions between the peptides. Since the A21G substitution extends the existing GxxxG repeat to include an extra repeat of the motif N-terminally compared to the WT, the d_{GG} value was recalculated using the G29 residues instead of G33. In the A21G system, both simulations that had yielded intermediate $d_{G33-G33}$ values were found to be stabilized primarily by G29 interactions (Fig. 6.2, bottom right), yielding two Gly-in structures (one right-handed and one left-handed), as well as left- and right-handed Gly-out structures.

To further examine specific interactions in each representative structure, the average ψ_{Crick} angles at each residue were calculated over the last 50 ns of the trajectory (Fig. 6.3). In the WT, the Gly-in structure is observed to be stabilized primarily by close interactions between residues G33 and G37. In the A21G mutant, however, this interaction shifts primarily to residues G29, especially in the left-handed structure. The Gly-out frames in both systems show more similarity, with all structures showing closer contacts along the G38xxxA42 interface reported in previous work [121].

6.3.3 A21G mutation reduces TM domain helicity

The helicity at each residue was calculated for simulations of each characteristic structure and plotted in Fig. 6.4. In the WT system, for both the Gly-in and Gly-side substates, at least one of the peptides maintains a helical juxtamembrane (JM) region, and both peptides have very stable TM helices. In the Gly-in substates in the A21G mutant system, however, the JM helicity is much less prominent. The predominant LH Gly-in structure also shows a sharp drop in helicity in one of the peptides at the G37/G38 kink as well as

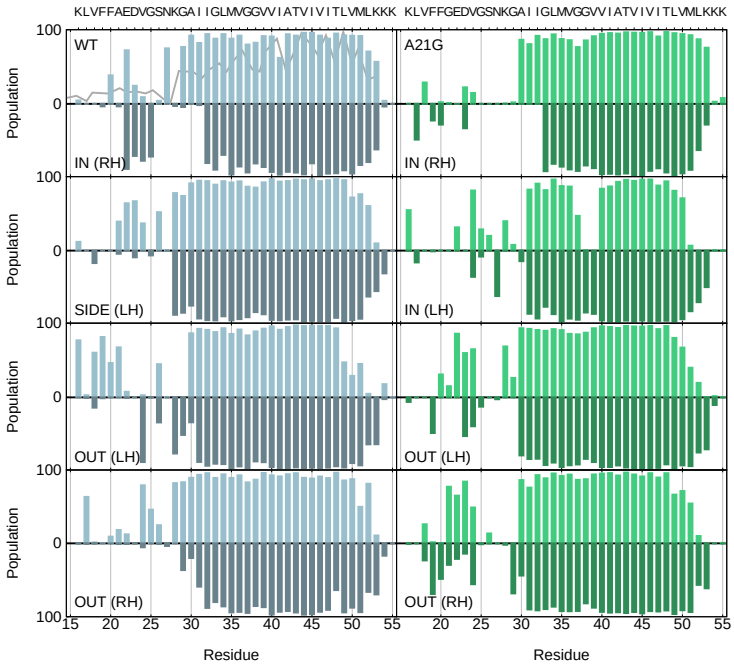

Figure 6.4: Helicity values for each residue derived from all-atom simulations of $C99_{15-55}$ homodimers in POPC bilayer for all structures in the WT system (left) and A21G system (right). Shades indicate respective peptides. Grey line indicates helicity values calculated from C_α chemical shift NMR data [67].

in the C-terminal domain, both sites of γ-processing.

This C-terminal drop in helicity is seen in one peptide in each of the A21G systems, beginning at residue V50, the common location of initial ϵ-cleavage by γ-secretase. This drop in helicity has been previously reported in the WT $C99_{15-55}$ system as a structural modification of the TM domain facilitating γ-processing [127]. The stability of the TM helix has been studied for its correlation to γ-cleavage, and it has been suggested that the loss of helical structure near processing sites allows for cleavage to occur [36]. It has also been posited that dimerization of the APP-C99 system increases the population of non-helical conformations in the C-terminal portion of the TM region, promoting peptide processing [29]. The prominence of this feature in the A21G system could make the mutant sequence more available for cleavage, explaining the observed increase in Aβ production.

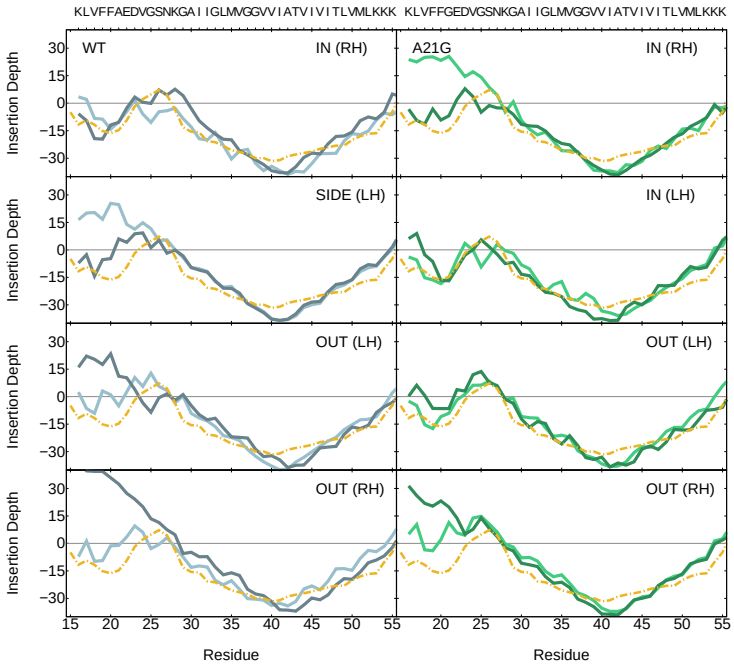

Figure 6.5: Membrane insertion depths of each residue derived from all-atom simulations of $C99_{15-55}$ homodimers in POPC bilayer for all structures in the WT system (left) and A21G system (right). Shades indicate depth of insertion derived from respective peptides in the homodimer. Orange dashed lines indicate experimental power saturation (EPR) measurements on WT C99 [90].

6.3.4 WT and A21G Gly-in structures display similar peptide positioning in lipid bilayer

The insertion depth of each residue was calculated by comparing the position along the membrane normal to the center of the surrounding lipid head group atoms (Fig. 6.5). Positive values indicate residues above the head group, while negative values indicate reinsertion into the lipid bilayer. In the WT sequence, the primary Gly-in structure displays reinsertion of the JM LVFFA region into the lipid bilayer in agreement with experimentally reported results [67, 92, 90]. In the other WT structures, however, one peptide shows moderate reinsertion of the JM region while the other extends from the membrane surface.

In the A21G mutant sequences, the primary structure (LH Gly-in) was also characterized by reinsertion of both peptides, while the RH Gly-in and Gly-out structures both contained

one peptide with an extended JM region. This suggests that the A21G substitution affects how the JM regions of the homodimers interact with each other and with the lipid bilayer, resulting in the changes to the interface seen in Fig. 6.3.

The systems only displayed slight differences in the kink and tilt angles of the peptides (Fig. 6.6). As was presented in previous studies on the WT $C99_{15-55}$ structure [121], the WT Gly-in structure is characterized by a right-handed structure featuring a tight coiled-coil interface stabilized by close GxxxG contacts along residues G33 and G37. The Gly-side structure commonly found in intermediate membrane widths has low kink and tilt values for both peptides in the homodimer, and the Gly-out structures (associated with narrow membrane environments and micelles [127]) are characterized by larger N-terminal tilt values.

The A21G LH Gly-in structure, which was similar to the WT in terms of the JM reinsertion (Fig. 6.5), is also characterized by an asymmetric homodimer, with one peptide characterized by a straighter, extended TM helix and the second complementary strand forming a prominent bend, facilitating close interpeptide interaction. This characteristic asymmetry is observed in both the WT and A21G mutant peptides (Fig. 6.7), despite the shift in the GxxxG interface. The sharp kink at residues G37/G38, causing a significant drop in the helical nature of the TM region (Fig. 6.4), is accompanied by the loss of close interpeptide contacts at residues G37 as well as G33, instead favoring contacts at residues G29 at the N-terminal interfacial region of the peptides.

6.4 Discussion

6.4.1 A21G mutation shifts GxxxG interface in $C99_{15-55}$ homodimers

The GxxxG repeat motifs in the TM sequence of APP have been of great interest as allowing for close interpeptide contacts facilitating dimerization of the APP strand [54, 53, 29]. It has been demonstrated experimentally as well as computationally that in the WT system

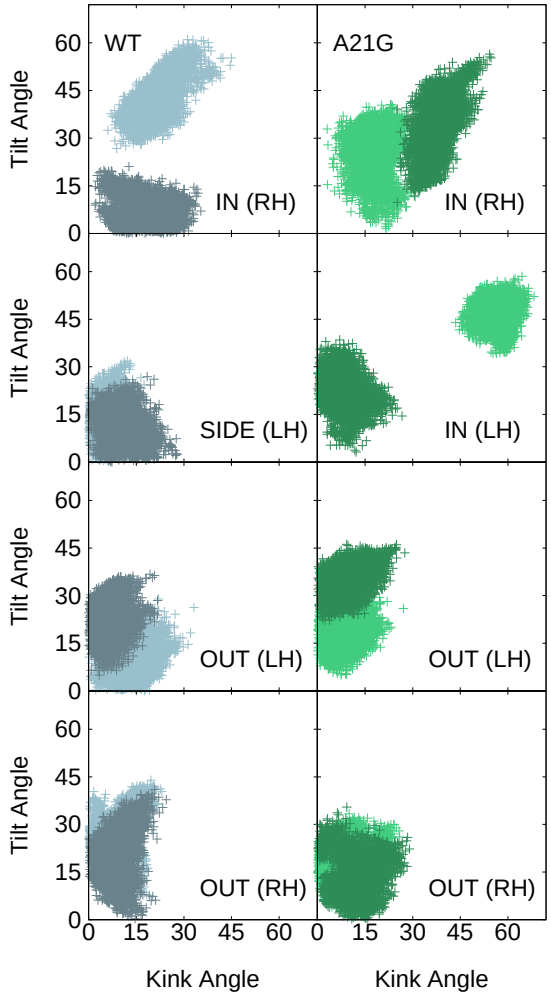

Figure 6.6: Peptide kink and N-terminal tilt angles derived from all-atom simulations of $C99_{15-55}$ homodimers in POPC bilayer for all structures in the WT system (left) and A21G system (right). Shades indicate respective peptides in the homodimer.

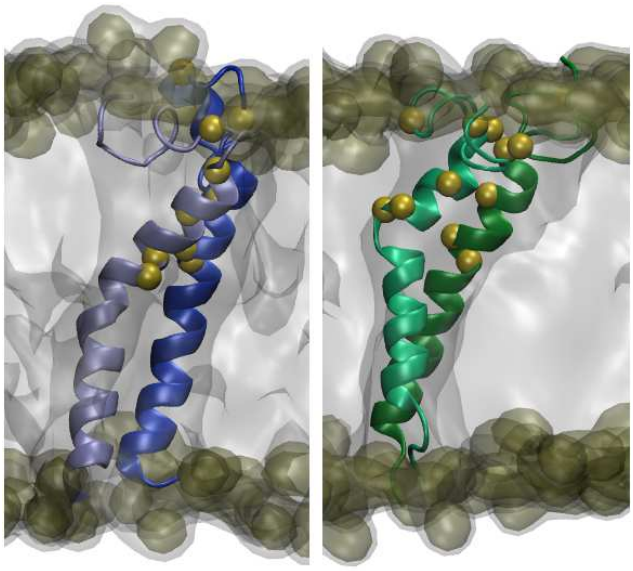

Figure 6.7: Representative structures of WT (left) and A21G (right) peptides derived from all-atom simulations of $C99_{15-55}$ homodimers in POPC bilayer. Yellow beads show the location of TM glycine residues. The lipid domain is marked as a translucent surface, with head group regions highlighted in dark yellow.

these contacts occur primarily at residues G33 and G37 [91, 100, 121]. The A21G mutation, however, extends the GxxxG repeat by one N-terminal motif, and it has been suggested that this mutation could be responsible for a change in the dimer interface [91]. In this study, the dominant form of the WT $C99_{15-55}$ homodimer is a right-handed Gly-in structure stabilized by close G33 and G37 contacts between peptides. In the A21G mutant system, however, the dominant structure is a left-handed Gly-in structure where the main interface has been shifted N-terminally to residues G29 on each peptide (Fig. 6.3).

It is also noted that while many differences are observed between the WT and A21G Gly-in structures (both LH and RH), the Gly-out structures for both systems show more similarities in terms of structural characteristics such as helicity, identity of residues forming the homodimer interface, as well as kink and tilt angles. The structures characterizing the $C99_{15-55}$ A21G mutant peptide homodimer ensemble are stabilized primarily along the G38xxxA42 interface described in previous studies [121, 91]. The similarities between these

structures suggests that the effect of the A21G mutation is specific primarily to the GxxxG interface motif.

6.4.2 A21G mutation alters TM peptide helicity

A21G substitution also led to a significant effect on the peptide helicity in $C99_{15-55}$ homodimers. Within the TM sequence, the A21G LH Gly-in structure is characterized by a large drop in helicity at residues G37/G38 due to an increase in the kink angle in one of the peptides (Figs. 6.4 and 6.6). In the JM region, the A21G mutation decreased helicity overall, although both peptides show helical population at residues V24/G25, whereas in the WT sequence, only one of the peptides contained helical content at these residues.

In both the WT and A21G systems it was observed that many structures were characterized by the C-terminal end of one peptide being less helical; a feature found to be more prominent in the A21G mutants. It has been suggested that homodimerization of APP-C99 stabilizes helicity in the N-terminal TM region while destabilizing helicity in the C-terminal domain near the ϵ-site, thereby facilitating γ-cleavage [29]. If this characteristic is enhanced by A21G mutation, as suggested by our simulation results, it could play a role in the increased γ-processing of the A21G mutants observed in previous studies [45, 126, 91]

6.4.3 Peptide positioning in lipid bilayer is only moderately affected by A21G mutation

Despite significant changes to the secondary structure and interpeptide contacts of the $C99_{15-55}$ homodimers, both the WT and A21G systems were found to have similar interactions with the lipid bilayer, as demonstrated by similar patterns of residue insertion depth as well as peptide kink and tilt angles within the POPC bilayer.

The predominant structure characterizing the homodimer ensemble of both sequences was characterized by reinsertion of the $L^{17}VFF^{20}$ region into the lipid bilayer (Fig. 6.5); a structural feature which our previous work has suggested might have a critical effect

on normal γ-processing[128]. For homodimers formed from the $C99_{15-55}$ WT or A21G sequences, the structures were found to be asymmetric, with one peptide forming a largely straight, extended TM helix and the complementary strand forming a prominent bend with much larger kink and tilt angles (Fig. 6.6). This structural feature was greatly enhanced in the A21G mutant homodimer, where the kink angle was up to 30 degrees larger than was found in the WT homodimer.

Chapter 7

Conclusion

7.1 Summary

The work presented here has explored fundamental aspects related to the structure and dynamics of C99 peptide monomer and homodimer, including dependence on sequence and membrane environment, that are critical to our understanding of the genesis of Aβ-peptide from the processing of APP-C99 by γ-secretase. By investigating a collection of systems consisting of fragments of C99 of varying length and sequence as well as in a variety of lipid environments, we addressed the following critical questions: What role does the sequence of APP play in the γ-processing pathway? How do both engineered and familial mutants affect the structure and interactions of C99 peptides, and how might those changes alter their subsequent processing? How sensitive are the structure and positioning of C99 monomers and dimers to their surrounding environment? How do changes in the environment alter the structure and especially the homodimer ensemble of APP-C99? Our main findings are presented here.

7.2 Key Findings

K28 mutations. The results presented in this study inform the following conclusions about $C99_{1-55}$ in a bilayer environment: (1) The WT $C99_{1-55}$ peptide is characterized by two dominant structural forms marked by a helical and β-structured JM domain, respectively. The existence of this ensemble suggests a flexible JM region, and provides support for experimental results that have shown the existence of both helical and β-structured forms. (2) The CHC of $C99_{1-55}$ independently adopts a helical structure or reinserts into the bilayer. This result extends the understanding developed in previous studies that posited

the existence of a helical CHC region and its reinsertion in the lipid bilayer. We find that the system exists as two distinct states (helical and non-helical), which may be dependent on both peptide sequence and lipid composition. (3) Mutations at K28 have a pronounced effect on the structural ensemble and positioning of the $C99_{1-55}$ peptide. These effects include destabilization of the salt-bridge formed between K28 and residues E22/D23, extension of the TM helix, as well as increased kink and tilt angles of the peptides within the bilayer. These results provide insight into structural changes in C99 that may underly changes in γ-processing of mutant peptides observed in previous works.

$C99_{15-55}$ homodimers. We find that the $C99_{15-55}$ system is best characterized by an ensemble of structural forms. (1) The C99 peptide contains three main helical regions: the TM region consisting of N-terminal and C-terminal helices, as well as a less-stable JM helix region. (2) The $C99_{15-55}$ ensemble also includes a variety of homodimer structures, characterized by different, distinct peptide interfacial regions. These features are best described by the relative location and orientation of the key residues G33 and G37 - part of the GxxxG repeat motif - as being Gly-in, Gly-side, or Gly-out, and include both left- and right-handed coiled-coil interactions between the peptides. (3) Clustering simulations according to local membrane character suggests a role for "environmental selection" of these different substates.

$C99_{23-55}$ homodimers in varying lipid environment. In agreement with our studies on $C99_{15-55}$ homodimers, we find that homodimers of the TM sequence of APP are characterized by an ensemble of forms which are highly sensitive to local membrane environment. (1) By simulating $C99_{23-55}$ homodimers in a variety of implicit and explicit lipid environments, we demonstrate a distinct shift in dimer interface as membrane width is varied. (2) While wider bilayer systems are characterized by predominantly right-handed Gly-in structures, narrowing the bilayer environment is found to shift sampling more heavily towards Gly-side and Gly-out structures. (3) While previous experimental studies have observed that varying lipid composition may [36] or may not [30] impact TM domain helic-

ity, the results of this study suggest that the TM domain helicity is not a sensitive function of lipid composition for the lipid bilayers studied. These findings can help explain the differences in experimentally-reported structures of APP-C99 dimers, which have been carried out in a variety of lipid and micelle environments.

FAD Flemish A21G mutation. The juxtamembrane region of APP-C99 has often been studied for its central importance as a precursor protein processed by γ-secretase to produce Aβ-peptide of central importance to AD [93]. In order to understand the relationship of sequence in the production of Aβ, there has been substantial interest in examining the impact of both FAD [44, 45, 126, 91] and engineered [46, 47, 48, 49, 50, 128] mutations on the processing of APP-C99 by γ-secretase. There has also been interest in the importance of TM helix stability in the availability and processing of APP-C99 [36, 29].

While many characterized FAD mutants have been shown to alter the ratio of Aβ42/Aβ40 [85, 87], the Flemish A21G mutation is thought to operate via a separate mechanism, leading to cerebral haemorrhage and early death [44]. This study examined the effect of A21G mutation on the structure and dimerization of APP-C99$_{15-55}$ peptides in order to provide insight into the role of FAD mutation on the structure and processing of APP-C99.

The results of our work lead to the following conclusions about the impact of the Flemish A21G FAD mutation: (1) The A21G substitution, which extends the well-known GxxxG repeat motif, extends the dimer interface from interpeptide contact at residues G33 and G37 to include residues G29. (2) The TM helicity of A21G mutant peptides is significantly lower both at the G37/G38 kink as well as at the C-terminal end of the homodimer, both locations of processing by γ-secretase. (3) Peptide positioning (characterized by residue insertion profiles as well as peptide kink/tilt angles) is only moderately affected by A21G mutation. Although it remains possible that the pathological effect of A21G substitution is caused by other effects - including direct interactions between the JM region and γ-secretase, which remains outside the scope of this work - this study provides valuable insight into the effect of this mutation on the structure and specific chemical interactions of the system.

7.3 Future Work

The studies presented here provide a foundation for future computational and experimental studies exploring the role of sequence and membrane in the structure and dynamics of C99 in lipid bilayers. While we have gained insight into the structure and dynamics of C99 monomer and homodimer, putative substrates for cleavage by γ-secretase, many questions remain surrounding specific details related to the interaction of C99 with γ-secretase, γ-cleavage and Aβ production. In particular, recent progress in the elucidation of a structural homologue to the presenilin active site domain of γ-secretase [129] has opened the door for computational studies investigating detailed intermolecular interactions between APP and the γ-secretase active site. Some early studies probing the interactions of C99 monomer with the homologue of presinilin have already been started in our lab, and we hope to see more work continue in this area.

A significant number of FAD mutants of C99, known to impact the cleavage of C99 by γ-secretase and the resulting Aβ product distribution, have been identified. It would be fruitful to apply the computational models developed and, to a degree, validated in the studies presented here to an expanded number of FAD mutant sequences, including representatives of the London and Florida FAD mutant peptides. Those additional studies promise to provide molecular-level insights into the changes in the structure of C99 monomer and homodimer induced by FAD mutations, which can help answer vital questions into the pathological effects of these single-site substitutions.

Finally, we hope that results presented here will inspire experimental work to provide a critical test of our findings related to the impact of varying sequence and membrane environment on C99 structure and dynamics, and to extend those results to provide insight into the relationship between C99 structure and activity, its cleavage by γ-secretase in the production of Aβ.

Bibliography

[1] K. A. Jellinger, "Alzheimer 100 - highlights in the history of Alzheimer research," *Journal of Neural Transmission*, vol. 113, pp. 1603–1623, 2006.

[2] R. Katzman, "Alzheimer's Disease," *The New England Journal of Medicine*, vol. 314, no. 15, pp. 964–973, 1986.

[3] R. D. Terry, N. K. Gonatas, and M. Weiss, "Ultrastructural Studies in Alzheimer's Presenile Dementia," *American Journal of Pathology*, vol. 44, no. 2, pp. 269–297, 1963.

[4] M. Kidd, "Paired Helical Filaments in Electron Microscopy of Alzheimer's Disease," *Nature*, vol. 197, pp. 192–193, 1963.

[5] G. G. Glenner and C. W. Wong, "Alzheimer's disease: Initial report of the purification and characterization of a novel cerebrovascular amyloid protein," *Biochemical and Biophysical Research Communications*, vol. 120, no. 3, pp. 885–890, 1984.

[6] D. M. Walsh, I. Klyubin, J. V. Fadeeva, W. K. Cullen, R. Anwyl, M. S. Wolfe, M. J. Rowan, and D. J. Selkoe, "Naturally secreted oligomers of amyloid β protein potently inhibit hippocampal long-term potentiation in vivo," *Nature*, vol. 416, pp. 535–539, 2002.

[7] T. Oltersdorf, P. J. Ward, T. Henriksson, E. C. Beattie, R. Neve, I. Lieberburg, and L. C. Fritz, "The Alzheimer Amyloid Precursor Protein. Identification of a stable intermediate in the biosynthetic/degradative pathway.," *Journal of Biological Chemistry*, vol. 265, pp. 4492–4497, 1990.

[8] J. Hardy and D. J. Selkoe, "The Amyloid Hypothesis of Alzheimer's Disease: Progress and Problems on the Road to Therapeutics," *Science*, vol. 297, pp. 353–356, 2002.

[9] J. Kang, H.-G. Lemaire, A. Unterbeck, J. M. Salbaum, C. L. Masters, K.-H. Grzeschik, G. Multhaup, K. Beyreuther, and B. Muller-Hill, "The precursor of Alzheimer's disease amyloid A4 protein resembles a cell-surface receptor," *Nature*, vol. 325, pp. 733–736, 02 1987.

[10] N. Kitaguchi, Y. Takahashi, Y. Tokushima, S. Shiojiri, and H. Ito, "Novel precursor of Alzheimer's disease amyloid protein shows protease inhibitory activity," *Nature*, vol. 331, pp. 530–532, 1988.

[11] P. Ponte, P. G. DeWhitt, J. Schilling, J. Miller, D. Hsu, B. Greenberg, K. Davis, W. Wallace, I. Lieberburg, F. Fuller, and B. Cordell, "A new A4 amyloid mRNA contains a domain homologous to serine proteinase inhibitors," *Nature*, vol. 331, pp. 525–527, 02 1988.

[12] R. J. O'Brien and P. C. Wong, "Amyloid Precursor Protein Processing and Alzheimer's Disease," *Annual Review of Neuroscience*, vol. 34, pp. 185–204, 2011.

[13] R. Postina, "A Closer Look at α-Secretase," *Current Alzheimer Research*, vol. 5, pp. 179–186, 2008.

[14] M. S. Wolfe and S. Y. Guénette, "APP at a glance," *Journal of Cell Science*, vol. 120, pp. 3157–3161, 2007.

[15] R. Vassar, B. D. Bennett, S. Babu-Khan, S. Kahn, E. A. Mediaz, P. Denis, D. B. Teplow, S. Ross, P. Amarante, R. Loeloff, Y. Luo, S. Fisher, J. Fuller, S. Edenson, J. Lile, M. A. Jarosinski, A. L. Biere, E. Curran, T. Burgess, J.-C. Louis, F. Collins, J. Treanor, G. Rogers, and M. Citron, "β-Secretase Cleavage of Alzheimer's Amyloid Precursor Protein by the Transmembrane Aspartic Protease BACE," *Science*, vol. 286, pp. 735–741, 1999.

[16] S. Sinha and I. Lieberburg, "Cellular mechanisms of β-amyloid production and secretion," *Proceedings of the National Academy of Sciences*, vol. 96, pp. 11049–11053, 1999.

[17] C. E. Hunt and A. J. Turner, "Cell biology, regulation and inhibition of β-secretase (BACE-1)," *Federation of European Biochemical Societies*, vol. 276, pp. 1845–1859, 2009.

[18] W. P. Esler, W. T. Kimberly, B. L. Ostaszewski, W. Ye, T. S. Diehl, D. J. Selkoe, and M. S. Wolfe, "Activity-dependent isolation of the presenilin γ-secretase complex reveals nicastrin and a γ substrate," *Proceedings of the National Academy of Sciences*, vol. 99, no. 5, pp. 2720–2725, 2002.

[19] S. Shah, S.-F. Lee, K. Tabuchi, Y.-H. Hao, C. Yu, Q. LaPlant, H. Ball, C. E. Dann III, T. Südhof, and G. Yu, "Nicastrin Functions as a Gamma-Secretase-Substrate Receptor," *Cell*, vol. 122, pp. 435–447, 2005.

[20] M. S. Wolfe, "The γ-Secretase Complex: Membrane-Embedded Proteolytic Ensemble," *Biochemistry*, vol. 45, no. 26, 2006.

[21] Y. Gu, H. Misonou, T. Sato, N. Dohmae, K. Takio, and Y. Ihara, "Distinct Intramembrane Cleavage of the β-Amyloid Precursor Protein Family Resembling γ-Secretase-like Cleavage of Notch," *Journal of Biological Chemistry*, vol. 276, pp. 35235–35238, 2001.

[22] M. Sastre, H. Steiner, K. Fuchs, A. Capell, G. Multhaup, M. M. Condron, D. B. Teplow, and C. Haass, "Presinilin-dependent γ-secretase processing of β-amyloid precursor protein at a site corresponding to the S3 cleavage of Notch," *European Molecular Biology Organization*, vol. 2, no. 9, pp. 835–841, 2001.

[23] C. Yu, S.-H. Kim, T. Ikeuchi, H. Xu, L. Gasparini, R. Wang, and S. S. Sisodia, "Characterization of a Presinilin-mediated Amyloid Precursor Protein Carboxyl-terminal

Fragment γ," *Journal of Biological Chemistry*, vol. 276, no. 47, pp. 43756–43760, 2001.

[24] A. Weidemann, S. Eggert, F. B. M. Reinhard, M. Vogel, K. Paliga, G. Baier, C. L. Masters, K. Beyreuther, and G. Evin, "A Novel ϵ-Cleavage within the Transmembrane Domain of the Alzheimer Amyloid Precursor Protein Demonstrates Homology with Notch Processing," *Biochemistry*, vol. 41, pp. 2825–2835, 2002.

[25] G. Zhao, G. Mao, J. Tan, Y. Dong, M.-Z. Cui, S.-H. Kim, and X. Xu, "Identification of a New Presenilin-dependent ζ-Cleavage Site within the Transmembrane Domain of Amyloid Precursor Protein," *Journal of Biological Chemistry*, vol. 279, no. 49, pp. 50647–50650, 2004.

[26] G. Zhao, M.-Z. Cui, G. Mao, Y. Dong, J. Tan, L. Sun, and X. Xu, "γ-Cleavage Is Dependent on ζ-Cleavage during the Proteolytic Processing of Amyloid Precursor Protein within Its Transmembrane Domain," *Journal of Biological Chemistry*, vol. 280, no. 45, pp. 37689–37697, 2005.

[27] S. Yagishita, M. Morishima-Kawashima, S. Ishiura, and Y. Ihara, "Aβ46 Is Processed to Aβ40 and Aβ43, but Not to Aβ42, in the Low Density Membrane Domains," *Journal of Biological Chemistry*, vol. 283, no. 2, pp. 733–788, 2008.

[28] Y. Qi-Takahara, M. Morishima-Kawashima, Y. Tanimura, G. Dolios, N. Hirotani, Y. Horikoshi, F. Kametani, M. Maeda, T. C. Saido, R. Wang, and Y. Ihara, "Longer Forms of Amyloid β Protein: Implications for the Mechanism of Intramembrane Cleavage by γ-Secretase," *Neurobiology of Disease*, vol. 35, no. 2, pp. 436–445, 2005.

[29] O. Pester, P. J. Barrett, D. Hornburg, P. Hornburg, R. Pröbstle, S. Widmaier, C. Kutzner, M. Dürrbaum, A. Kapurniotu, C. R. Sanders, C. Scharnagl, and D. Langosch, "The Backbone Dynamics of the Amyloid Precursor Protein Transmembrane

Helix Provides a Rationale for the Sequential Cleavage Mechanism of γ-Secretase," *Journal of the American Chemical Society*, vol. 135, no. 4, pp. 1317–1329, 2013.

[30] A. J. Beel and C. R. Sanders, "Substrate specificity of gamma-secretase and other intramembrane proteases," *Cellular and Molecular Life Sciences*, vol. 65, pp. 1311–1334, 2008.

[31] G. Bitan, M. D. Kirkitadze, A. Lomakin, S. S. Vollers, G. B. Benedek, and D. B. Teplow, "Amyloid β-protein (Aβ) assembly: Aβ40 and Aβ42 oligomerize through distinct pathways," *Proceedings of the National Academy of Sciences*, vol. 100, no. 1, pp. 330–335, 2003.

[32] Y.-R. Chen and C. G. Glabe, "Distinct Early Folding and Aggregation Properties of Alzheimer Amyloid-β Peptides Aβ40 and Aβ42," *Journal of Biological Chemistry*, vol. 281, no. 34, pp. 24414–24422, 2006.

[33] A. Weihofen and B. Martoglio, "Intramembrane-cleaving proteases: controlled liberation of proteins and bioactive peptides," *TRENDS in Cell Biology*, vol. 13, no. 2, pp. 71–78, 2003.

[34] M. S. Wolfe and R. Kopan, "Intramembrane Proteolysis: Theme and Variations," *Science*, vol. 305, pp. 1119–1123, 2004.

[35] R. Kopan and M. X. G. Ilagan, "γ-Secretase: proteasome of the membrane?," *Nature Reviews*, vol. 5, pp. 499–504, 2004.

[36] J.-X. Lu, W.-M. Yau, and R. Tycko, "Evidence from Solid-State NMR for Nonhelical Conformations in the Transmembrane Domain of the Amyloid Precursor Protein," *Biophysical Journal*, vol. 100, pp. 711–719, 2011.

[37] O. Quintero-Monzon, M. M. Martin, M. A. Fernandez, C. A. Cappello, A. J. Krzysiak, P. Osenkowski, and M. S. Wolfe, "Dissociation between the Processivity and Total Ac-

tivity of γ-Secretase: Implications for the Mechanism of Alzheimer's Disease-Causing Presinilin Mutations," *Biochemistry*, vol. 50, pp. 9023–9035, 2011.

[38] M. Simons, P. Keller, B. de Strooper, K. Beyreuther, C. G. Dotti, and K. Simons, "Cholesterol depletion inhibits the generation of β-amyloid in hippocampal neurons," *Proceedings of the National Academy of Sciences*, vol. 95, pp. 6460–6464, 1998.

[39] S. Wahrle, P. Das, A. C. Nyborg, C. McLendon, M. Shoji, T. Kawarabayashi, L. H. Younkin, S. G. Younkin, and T. E. Golde, "Cholesterol-Dependent γ-Secretase Activity in Buoyant Cholesterol-Rich Membrane Microdomains," *Neurobiology of Disease*, vol. 9, pp. 11–23, 2002.

[40] A. Goate, M.-C. Chartier-Harlin, M. Mullan, J. Brown, F. Crawford, L. Fidani, L. Giuffra, A. Haynes, N. Irving, L. James, R. Mant, P. Newton, K. Rooke, P. Roques, C. Talbot, M. Pericak-Vance, A. Roses, R. Williamson, M. Rossor, M. Owen, and J. Hardy, "Segregation of a missense mutation in the amyloid precursor protein gene with familial Alzheimer's disease," *Nature*, vol. 349, pp. 704–706, 1991.

[41] M.-C. Chartier-Harlin, F. Crawford, K. Hamandi, M. Mullan, A. Goate, J. Hardy, H. Backhovens, J.-J. Martin, and C. V. Broeckhoven, "Screening for the β-amyloid precursor protein mutation (APP717:Val→Ile) in extended pedigrees with early onset Alzheimer's disease," *Neuroscience Letters*, vol. 129, pp. 134–135, 1991.

[42] R. E. Tanzi, G. Vaula, D. M. Romano, M. Mortilla, T. L. Huang, R. G. Tupler, W. Wasco, B. T. Hyman, J. L. Haines, B. J. Jenkins, M. Kalaitsidaki, A. C. Warren, M. C. McInnis, S. E. Antonarakis, H. Karlinsky, M. E. Percy, L. Connor, J. Growdon, D. R. Crapper-Mclachlan, J. F. Gusella, and P. H. S. George-Hyslop, "Assessment of Amyloid β-Protein Precursor Gene Mutations in a Large Set of Familial and Sporadic Alzheimer Disease Cases," *American Journal of Human Genetics*, vol. 51, pp. 273–282, 1992.

[43] M. Mullan, F. Crawford, K. Axelman, H. Houlden, L. Lilius, B. Winblad, and L. Lannfelt, "A pathogenic mutation for probable Alzheimer's disease in the APP gene at the N-terminus of β-amyloid," *Nature Genetics*, vol. 1, pp. 345–347, 1992.

[44] L. Hendriks, C. M. van Duijn, P. Cras, M. Cruts, W. V. Hul, F. van Harskamp, A. Warren, M. G. McInnis, S. E. Antonarakis, J.-J. Martin, A. Hofman, and C. V. Broeckhoven, "Presenile dementia and cerebral haemorrhage linked to a mutation at codon 692 of the β-amyloid precursor protein gene," *Nature Genetics*, vol. 1, pp. 218–221, 1992.

[45] C. D. Jonghe, C. Zehr, D. Yager, C.-M. Prada, S. Younkin, L. Hendriks, C. V. Broeckhoven, and C. B. Eckman, "Flemish and Dutch Mutations in Amyloid β Precursor Protein Have Different Effects on Amyloid β Secretion," *Neurobiology of Disease*, vol. 5, no. 4, pp. 281 – 286, 1998.

[46] Z. Ren, D. Schenk, G. S. Basi, and I. P. Shapiro, "Amyloid β-Protein Precursor Juxtamembrane Domain Regulates Specificity of γ-Secretase-dependent Cleavages," *Journal of Biological Chemistry*, vol. 282, no. 48, pp. 35350–35360, 2007.

[47] R. M. Page, A. Gutsmiedl, A. Fukumori, E. Winkler, C. Haass, and H. Steiner, "β-Amyloid Precursor Protein Mutants Respond to γ-Secretase Modulators," *Journal of Biological Chemistry*, vol. 285, no. 23, pp. 17798–17810, 2010.

[48] T. L. Kukar, T. B. Ladd, P. Robertson, S. A. Pintchovski, B. Moore, M. A. Bann, Z. Ren, K. Jansen-West, K. Malphrus, S. Eggert, H. Maruyama, B. A. Cottrell, P. Das, G. S. Basi, E. H. Koo, and T. E. Golde, "Lysine 624 of the Amyloid Precursor Protein (APP) is a Critical Determinant of Amyloid Beta Peptide Length: Support for a sequential model of γ-secretase intramembrane proteolysis and regulation by the APP juxtamembrane region.," *Journal of Biological Chemistry*, 2011.

[49] S. Ousson, A. Saric, A. Baguet, C. Losberger, S. Genoud, F. Vilbois, B. Permanne, I. Hussain, and D. Beher, "Substrate determinants in the C99 juxtamembrane domains differentially affect γ–secretase cleavage specificity and modulator pharmacology," *Journal of Neurochemistry*, vol. 125, no. 4, pp. 610–619, 2013.

[50] J. I. Jung, Y. Ran, P. E. Cruz, A. M. Rosario, T. B. Ladd, T. L. Kukar, E. H. Koo, K. M. Felsenstein, and T. E. Golde, "Complex Relationships between Substrate Sequence and Sensitivity to Alterations in γ-Secretase Processivity Induced by γ-Secretase Modulators," *Biochemistry*, vol. 53, no. 12, pp. 1947–1957, 2014.

[51] S. Scheuermann, B. Hambsch, L. Hesse, J. Stumm, C. Schmidt, D. Beher, T. A. Bayer, K. Beyreuther, and G. Multhaup, "Homodimerization of Amyloid Precursor Protein and Its Implication in the Amyloidogenic Pathway of Alzheimer's Disease," *Journal of Biological Chemistry*, vol. 276, no. 36, pp. 33923–33929, 2001.

[52] P. Soba, S. Eggert, K. Wagner, H. Zentgraf, K. Siehl, S. Kreger, A. Lower, A. Langer, G. Merdes, R. Paro, C. L. Masters, U. Muller, S. Kins, and K. Beyreuther, "Homo- and heterodimerization of APP family members promotes intercellular adhesion," *The EMBO Journal*, vol. 24, pp. 3624–3634, 2005.

[53] P. M. Gorman, S. Kim, M. Guo, R. A. Melnyk, J. McLaurin, P. E. Fraser, J. U. Bowie, and A. Chakrabartty, "Dimerization of the transmembrane domain of amyloid precursor proteins and familial Alzheimer's disease mutants," *BMC Neuroscience*, vol. 9, 2008.

[54] L.-M. Munter, P. Voigt, A. Harmeier, D. Kaden, K. E. Gottschalk, C. Weise, R. Pipkorn, M. Schaefer, D. Langosch, and G. Multhaup, "GxxxG motifs within the amyloid precursor protein transmembrane sequence are critical for the etiology of Aβ42," *The EMBO Journal*, vol. 26, no. 6, pp. 1702–1712, 2007.

[55] S. Eggert, B. Midthune, B. Cottrell, and E. H. Koo, "Induced Dimerization of the Amyloid Precursor Protein Leads to Decreased Amyloid-β Protein Production," *Journal of Biological Chemistry*, vol. 284, no. 42, pp. 28943–28952, 2009.

[56] W. P. Russ and D. M. Engelman, "The GxxxG Motif: A Framework for Transmembrane Helix-Helix Association," *Journal of Molecular Biology*, vol. 296, pp. 911–919, 2000.

[57] Y. Sugita and Y. Okamoto, "Replica-exchange molecular dynamics method for protein folding," *Chemical Physics Letters*, vol. 314, p. 141, 1999.

[58] W. Im, M. S. Lee, and C. L. B. III, "Generalized Born Model with a Simple Smoothing Function," *Journal of Computational Chemistry*, vol. 24, pp. 1691–1702, 2003.

[59] S. J. Marrink, H. J. Risselada, S. Yefimov, D. P. Tieleman, and A. H. de Vries, "The martini force field: coarse grained model for biomolecular simulations," *Journal of Physical Chemistry B*, vol. 111, no. 27, pp. 7812–7824, 2007.

[60] L. Monticelli, S. K. Kandasamy, X. Periole, R. G. Larson, D. P. Tieleman, and S.-J. Marrink, "The martini coarse-grained force field: extension to proteins," *Journal of Chemical Theory and Computation*, vol. 4, no. 5, pp. 819–834, 2008.

[61] G. S. Ayton and G. A. Voth, "Systematic multiscale simulation of membrane protein systems," *Current Opinion in Structural Biology*, vol. 19, no. 2, pp. 138–144, 2009.

[62] A. P. Lyubartsev and A. L. Rabinovich, "Recent development in computer simulations of lipid bilayers," *Soft Matter*, vol. 7, no. 1, pp. 25–39, 2011.

[63] S. J. Marrink, A. H. de Vries, and D. P. Tieleman, "Lipids on the move: simulations of membrane pores, domains, stalks and curves," *Biochimica, Biophysica Acta - Biomembranes*, vol. 1788, no. 1, pp. 149–168, 2009.

[64] H. L. Scott, "Modeling the lipid component of membranes," *Current Opinion in Structural Biology*, vol. 12, no. 4, pp. 495–502, 2002.

[65] E. Psachoulia, P. W. Fowler, P. J. Bond, and M. S. Sansom, "Helix- helix interactions in membrane proteins: Coarse-grained simulations of glycophorin a helix dimerization†," *Biochemistry*, vol. 47, no. 40, pp. 10503–10512, 2008.

[66] J. M. Cuthbertson, P. J. Bond, and M. S. Sansom, "Transmembrane helix-helix interactions: comparative simulations of the glycophorin a dimer," *Biochemistry*, vol. 45, no. 48, pp. 14298–14310, 2006.

[67] A. J. Beel, C. K. Mobley, H. J. Kim, F. Tian, A. Hadziselimovic, B. Jap, J. H. Prestegard, and C. R. Sanders, "Structural Studies of the Transmembrane C-Terminal Domain of the Amyloid Precursor Protein (APP): Does APP Function as a Cholesterol Sensor?," *Biochemistry*, vol. 47, pp. 9428–9446, 2008.

[68] W. Humphrey, A. Dalke, and K. Schulten, "VMD – Visual Molecular Dynamics," *Journal of Molecular Graphics*, vol. 14, pp. 33–38, 1996.

[69] B. R. Brooks, R. E. Bruccoleri, B. D. Olafson, D. J. States, S. Swaminathan, and M. Karplus, "CHARMM: A program for macromolecular energy, minimization, and dynamics calculations," *Journal of Computational Chemistry*, vol. 4, no. 2, pp. 187–217, 1983.

[70] A. D. M. Jr., M. Feig, and C. L. B. III, "Extending the Treatment of Backbone Energetics in Protein Force Fields: Limitations of Gas-Phase Quantum Mechanics in Reproducing Protein Conformational Distributions in Molecular Dynamics Simulations," *Journal of Computational Chemistry*, vol. 25, pp. 1400–1415, 2004.

[71] J. Chen, W. Im, and C. L. B. III, "Balancing Solvation and Intramolecular Interactions: Toward a Consistent Generalized Born Force Field," *Journal of the American Chemical Society*, vol. 128, no. 11, pp. 3728–3736, 2006.

[72] M. Feig, J. Karanicolas, and C. L. B. III, "MMTSB Tool Set: enhanced sampling and multiscale modeling methods for applications in structural biology," *Journal of Molecular Graphics and Modelling*, vol. 22, pp. 377–395, 2004.

[73] S. Jo, T. Kim, V. Iyer, and W. Im, "CHARMM-GUI: A Web-based Graphical User Interface for CHARMM," *Journal of Computational Chemistry*, vol. 29, pp. 1859–1865, 2008.

[74] E. Wu, X. Cheng, S. Jo, H. Rui, K. Song, E. Dávila-Contreras, Y. Qi, J. Lee, V. Monje-Galvan, R. Venable, J. Klauda, and W. Im, "CHARMM-GUI Membrane Builder Toward Realistic Biological Membrane Simulations," *Journal of Computational Chemistry*, vol. 35, no. 27, pp. 1997–2004, 2014.

[75] S. Jo, T. Kim, and W. Im, "Automated builder and database of protein/membrane complexes for molecular dynamics simulations," *PLoS ONE*, vol. 2, p. e880, 09 2007.

[76] D. Van Der Spoel, E. Lindahl, B. Hess, G. Groenhof, A. E. Mark, and H. J. Berendsen, "GROMACS: fast, flexible, and free," *Journal of Computational Chemistry*, vol. 26, no. 16, pp. 1701–1718, 2005.

[77] B. Hess, C. Kutzner, D. Van Der Spoel, and E. Lindahl, "GROMACS 4: Algorithms for highly efficient, load-balanced, and scalable molecular simulation," *Journal of Chemical Theory and Computation*, vol. 4, no. 3, pp. 435–447, 2008.

[78] A. D. MacKerell, D. Bashford, M. Bellott, R. Dunbrack, J. Evanseck, M. J. Field, S. Fischer, J. Gao, H. Guo, S. a. Ha, *et al.*, "All-atom empirical potential for molecular modeling and dynamics studies of proteins," *Journal of Physical Chemistry B*, vol. 102, no. 18, pp. 3586–3616, 1998.

[79] J. B. Klauda, R. M. Venable, J. A. Freites, J. W. O'Connor, D. J. Tobias, C. Mondragon-Ramirez, I. Vorobyov, A. D. MacKerell Jr, and R. W. Pastor, "Update

of the CHARMM all-atom additive force field for lipids: validation on six lipid types," *Journal of Physical Chemistry B*, vol. 114, no. 23, pp. 7830–7843, 2010.

[80] W. G. Hoover, "Canonical dynamics: Equilibrium phase-space distributions," *Physical Reviews A*, vol. 31, no. 3, p. 1695, 1985.

[81] C. Haass and D. J. Selkoe, "Soluble protein oligomers in neurodegeneration: lessons from the Alzheimer's amyloid β-peptide," *Nature Reviews*, vol. 8, pp. 101–112, 2007.

[82] K. N. Dahlgren, A. M. Manelli, J. W. Blaine Stine, L. K. Baker, G. A. Krafft, and M. J. Ladu, "Oligomeric and Fibrillar Species of Amyloid-β Peptides Differentially Affect Neuronal Viability," *Journal of Biological Chemistry*, vol. 277, pp. 32046–32053, 2002.

[83] S. Parvathy, I. Hussain, E. H. Karran, A. J. Turner, and N. M. Hooper, "Cleavage of Alzheimer's Amyloid Precursor Protein by α-Secretase Occurs at the Surface of Neuronal Cells," *Biochemistry*, vol. 38, pp. 9728–9734, 1999.

[84] C. D. Jonghe, C. Esselens, S. Kumar-Singh, K. Craessaerts, S. Serneels, F. Checler, W. Annaert, C. V. Broeckhoven, and B. D. Strooper, "Pathogenic APP mutations near the γ-secretase cleavage site differentially affect Aβ secretion and APP C-terminal fragment stability," *Human Molecular Genetics*, vol. 10, no. 16, pp. 1665–1671, 2001.

[85] C. B. Eckman, N. D. Mehta, R. Crook, J. Perez-tur, G. Prihar, E. Pfeiffer, N. Graff-Radford, P. Hinder, D. Yager, B. Zenk, L. M. Refolo, C. M. Prada, S. G. Younkin, M. Hutton, and J. Hardy, "A new pathogenic mutation in the APP gene (I716V) increases the relative proportion of Aβ42(43)," *Human Molecular Genetics*, vol. 6, no. 12, pp. 2087–2089, 1997.

[86] J. B. J. Kwok, Q.-X. Li, M. Hallupp, S. Whyte, D. Ames, K. Beyreuther, C. L. Masters, and P. R. Schofield, "Novel Leu723Pro Amyloid Precursor Protein Muta-

tion Increases Amyloid β42(43) Peptide Levels and Induces Apoptosis," *Annals of Neurology*, vol. 47, pp. 249–253, 2000.

[87] S. F. Lichtenthaler, N. Ida, G. Multhaup, C. L. Masters, and K. Beyreuther, "Mutations in the Transmembrane Domain of APP Altering γ-Secretase Specificity," *Biochemistry*, vol. 36, pp. 15396–15403, 1997.

[88] K. L. Sciarretta, D. J. Gordon, A. T. Petkova, R. Tycko, and S. C. Meredith, "Aβ40-Lactam(D23/K28) Models a Conformation Highly Favorable for Nucleation of Amyloid," *Biochemistry*, vol. 44, pp. 6003–6014, 2005.

[89] G. Reddy, J. E. Straub, and D. Thirumalai, "Influence of Preformed Asp23-Lys28 Salt Bridge on the Conformational Fluctuations of Monomers and Dimers of Aβ Peptides with Implications for Rates of Fibril Formation," *Journal of Physical Chemistry B*, vol. 113, pp. 1162–1172, 2009.

[90] P. J. Barrett, Y. Song, W. D. V. Horn, E. J. Hustedt, J. M. Schafer, A. Hadziselimovic, A. J. Beel, and C. R. Sanders, "The Amyloid Precursor Protein has a Flexible Transmembrane Domain and Binds Cholesterol," *Science*, vol. 336, pp. 1168–1171, 2012.

[91] T.-C. Tang, Y. Hu, P. Kienlen-Campard, L. E. Haylani, M. Decock, J. V. Hees, Z. Fu, J.-N. Octave, S. N. Constantinescu, and S. O. Smith, "Comformation Changes Induced by the A21G Flemish Mutation in the Amyloid Precursor Protein Lead to Increased Aβ Production," *Structure*, vol. 22, 2014.

[92] K. D. Nadezhdin, O. V. Bocharova, E. V. Bocharov, and A. S. Arseniev, "Dimeric structure of transmembrane domain of amyloid precursor protein in micellar environment," *Federation of European Biochemical Societies Letters*, vol. 586, no. 12, pp. 1687–1692, 2012.

[93] J. Zhang, W. Ye, R. Wang, M. S. Wolfe, B. D. Greenberg, and D. J. Selkoe, "Proteolysis of Chimeric β-Amyloid Precursor Proteins Containing the Notch Transmembrane

Domain Yields Amyloid β-like Peptides," *Journal of Biological Chemistry*, vol. 277, no. 17, pp. 15069–15075, 2002.

[94] W. P. Esler and M. S. Wolfe, "A Portrait of Alzheimer Secretases – New Features and Familiar Faces," *Science*, vol. 293, p. 1449, 2001.

[95] G. Zhao, J. Tan, G. Mao, M.-Z. Cui, and X. Xu, "The same γ-secretase accounts for the multiple intramembrane cleavages of app," *Journal of Neurochemistry*, vol. 100, no. 5, pp. 1234–1246, 2007.

[96] P. Kienlen-Campard, B. Tasiaux, J. Van Hees, M. Li, S. Huysseune, T. Sato, J. Z. Fei, S. Aimoto, P. J. Courtoy, and S. O. Smith, "Amyloidogenic processing but not amyloid precursor protein (app) intracellular c-terminal domain production requires a precisely oriented app dimer assembled by transmembrane gxxxg motifs," *Journal of Biological Chemistry*, vol. 283, no. 12, pp. 7733–7744, 2008.

[97] L.-M. Munter, A. Botev, L. Richter, P. W. Hildebrand, V. Althoff, C. Weise, D. Kaden, and G. Multhaup, "Aberrant app processing in hereditary forms of alzheimer disease caused by app-fad mutations can be rescued by mutations in the app gxxxg motif," *Journal of Biological Chemistry*, 2010.

[98] T. Sato, T.-c. Tang, G. Reubins, J. Z. Fei, T. Fujimoto, P. Kienlen-Campard, S. N. Constantinescu, J.-N. Octave, S. Aimoto, and S. O. Smith, "A helix-to-coil transition at the ϵ-cut site in the transmembrane dimer of the amyloid precursor protein is required for proteolysis," *Proceedings of the National Academy of Sciences*, vol. 106, no. 5, pp. 1421–1426, 2009.

[99] J. H. Goo and W. J. Park, "Elucidation of the interactions between c99, presenilin, and nicastrin by the split-ubiquitin assay," *DNA and Cell Biology*, vol. 23, no. 1, pp. 59–65, 2004.

[100] N. Miyashita, J. E. Straub, D. Thirumalai, and Y. Sugita, "Transmembrane Structures of Amyloid Precursor Protein Dimer Predicted by Replica-Exchange Molecular Dynamics Simulations," *Journal of the American Chemical Society*, vol. 131, pp. 3438–3439, 2009.

[101] H. Wang, L. Barreyro, D. Provasi, I. Djemil, C. Torres-Arancivia, M. Filizola, and I. Ubarretxena-Belandia, "Molecular determinants and thermodynamics of the amyloid precursor protein transmembrane domain implicated in Alzheimer's disease," *Journal of Molecular Biology*, vol. 408, no. 5, pp. 879–895, 2011.

[102] W. Chen, M. Lopez, E. Gamache, Y. Li, and C. Wang, "Solution NMR structure of transmembrane domain of amyloid precursor protein WT." PDB ID: 2LZ3.

[103] L. Monticelli, S. K. Kandasamy, X. Periole, R. G. Larson, D. P. Tieleman, and S.-J. Marrink, "The martini coarse-grained force field: extension to proteins," *Journal of Chemical Theory and Computation*, vol. 4, no. 5, pp. 819–834, 2008.

[104] R. P and S. J, "Fast procedure for reconstruction of full-atom protein models from reduced representations," *Journal of Computational Chemistry*, vol. 29, pp. 1460–5, 2008.

[105] M. Feig, J. Karanicolas, and C. L. Brooks III, "MMTSB Tool Set," *MMTSB NIH Research Resource, The Scripps Research Institute*, 2001.

[106] H. J. Berendsen, J. P. M. Postma, W. F. van Gunsteren, A. DiNola, and J. Haak, "Molecular dynamics with coupling to an external bath," *Journal of Chemical Physics*, vol. 81, p. 3684, 1984.

[107] U. Essmann, L. Perera, M. L. Berkowitz, T. Darden, H. Lee, and L. G. Pedersen, "A smooth particle mesh ewald method," *Journal of Chemical Physics*, vol. 103, no. 19, pp. 8577–8593, 1995.

[108] B. Hess, H. Bekker, H. J. Berendsen, and J. G. Fraaije, "Lincs: a linear constraint solver for molecular simulations," *Journal of Computational Chemistry*, vol. 18, no. 12, pp. 1463–1472, 1997.

[109] W. Kabsch and C. Sander, "Dictionary of Protein Secondary Structure: Pattern Recognition of Hydrogen-Bonded and Geometrical Features," *Biopolymers*, vol. 22, pp. 2577–2637, 1983.

[110] R. P. Joosten, T. A. te Beek, E. Krieger, M. L. Hekkelman, R. W. Hooft, R. Schneider, C. Sander, and G. Vriend, "A series of pdb related databases for everyday needs," *Nucleic Acids Research*, vol. 39, no. suppl 1, pp. D411–D419, 2011.

[111] N. Michaud-Agrawal, E. J. Denning, T. B. Woolf, and O. Beckstein, "Mdanalysis: A toolkit for the analysis of molecular dynamics simulations," *Journal of Computational Chemistry*, vol. 32, no. 10, pp. 2319–2327, 2011.

[112] F. H. C. Crick, "The Packing of α-Helices: Simple Coiled-Coils," *Acta Crystallographica*, vol. 6, pp. 689–697, 1953.

[113] S. V. Strelkov and P. Burkhard, "Analysis of α-helical coiled coils with the program twister reveals a structural mechanism for stutter compensation," *Journal of Structural Biology*, vol. 137, pp. 54–64, 2002.

[114] A. N. Lupas and M. Gruber, "The structure of α-helical coiled coils," in *Fibrous Proteins: Coiled-Coils, Collagen and Elastomers* (D. A. D. Parry and J. M. Squire, eds.), vol. 70 of *Advances in Protein Chemistry*, pp. 37 – 38, Academic Press, 2005.

[115] K. R. MacKenzie, J. H. Prestegard, and D. M. Engelman, "A transmembrane helix dimer: structure and implications," *Science*, vol. 276, no. 5309, pp. 131–133, 1997.

[116] W. Chen, E. Gamache, D. J. Rosenman, J. Xie, M. M. Lopez, Y.-M. Li, and C. Wang, "Familial alzheimer's mutations within apptm increase aβ42 production by enhancing accessibility of ε-cleavage site," *Nature communications*, vol. 5, 2014.

[117] M. Lemmon, J. M. Flanagan, J. F. Hunt, B. D. Adair, B. Bormann, C. E. Dempsey, and D. Engelman, "Glycophorin a dimerization is driven by specific interactions between transmembrane alpha-helices.," *Journal of Biological Chemistry*, vol. 267, no. 11, pp. 7683–7689, 1992.

[118] A. Senes, D. E. Engel, and W. F. DeGrado, "Folding of helical membrane proteins: the role of polar, gxxxg-like and proline motifs," *Current Opinion in Structural Biology*, vol. 14, no. 4, pp. 465–479, 2004.

[119] P. J. Bond and M. S. P. Sansom, "Membrane Protein Dynamics *versus* Environment: Simulations of OmpA in a Micelle and in a Bilayer," *Journal of Molecular Biology*, vol. 329, no. 5, pp. 1035–1053, 2003.

[120] G. Patargias, P. J. Bond, S. S. Deol, and M. S. P. Sansom, "Molecular Dynamics Simulations of GlpF in a Micelle vs in a Bilayer: Conformational Dynamics of a Membrane Protein as a Function of Environment," *Journal of Physical Chemistry B*, vol. 109, no. 1, pp. 575–582, 2005.

[121] L. Dominguez, L. Foster, S. C. Meredith, J. E. Straub, and D. Thirumalai, "Structural Heterogeneity in Transmembrane Amyloid Precursor Protein Homodimer is a Consequence of Environmental Selection," *Journal of the American Chemical Society*, vol. 136, pp. 9619–9626, 2014.

[122] A. D. MacKerell, D. Bashford, M. Bellott, R. Dunbrack, J. Evanseck, M. J. Field, S. Fischer, J. Gao, H. Guo, S. a. Ha, *et al.*, "All-atom empirical potential for molecular modeling and dynamics studies of proteins," *Journal of Physical Chemistry B*, vol. 102, no. 18, pp. 3586–3616, 1998.

[123] D. Langosch and J. Heringa, "Interaction of Transmembrane Helices by a Knobs-Into-Holes Packing Characteristic of Soluble Coiled Coils," *Proteins: Structure, Function, and Genetics*, vol. 31, pp. 150–159, 1998.

[124] M. M. Javadpour, M. Eilers, M. Groesbeek, and S. O. Smith, "Helix Packing in Polytopic Membrane Proteins: Role of Glycine in Transmembrane Helix Association," *Biophysical Journal*, vol. 77, pp. 1609–1618, 1999.

[125] P. Burkhard, J. Stetefeld, and S. V. Strelkov, "Coiled coils: a highly versatile folding motif," *TRENDS in Cell Biology*, vol. 11, no. 2, pp. 82–88, 2001.

[126] Y. Tian, B. Bassit, D. Chau, and Y.-M. Li, "An APP inhibitory domain containing the Flemish mutation residue modulates γ-secretase activity for Aβ production," *Nature Structural and Molecular Biology*, vol. 17, pp. 151–158, 02 2010.

[127] L. Dominguez, S. C. Meredith, J. E. Straub, and D. Thirumalai, "Transmembrane Fragment Structures of Amyloid Precursor Protein Depend on Membrane Surface Curvature," *Journal of the American Chemical Society*, vol. 136, pp. 854–857, 2014.

[128] L. Foster and J. E. Straub, "Engineered mutations to residue K28 affect the structure and positioning of APP-C99 peptide in lipid bilayer: Implications for processing by γ-secretase.," *in preparation*, 2014.

[129] X. Li, S. Dang, C. Yan, X. Gong, J. Wang, and Y. Shi, "Structure of a presenilin family intermembrane aspartate protease," *Nature*, vol. 493, pp. 56–61, 2013.

Curriculum Vitae

Leigh Suzanne Holmes Foster, 1987

Boston University Department of Chemistry

590 Commonwealth Avenue, Room 299

Boston, MA 02215

Education

- Ph.D., Computational Chemistry, **Boston University**, Dissertation: The Effect of Sequence and Environment on the Structure and Dimerization of Amyloid Precursor Protein, January 2015
- M.A., Computational Chemistry, **Boston University**, May 2010
- B.A., Chemistry, **Mount Holyoke College**, Minor in Computer Science, May 2008 (*Magna Cum Laude with Honors*)

Publications

- "Comparison of proton conduction in $KTaO_3$ and $SrZrO_3$" Maria A. Gomez, Saryu Jindal, Katharyn M. Fletcher, Leigh S. Foster, and Nanna Dufie Addo. et al *Journal of Chemical Physics*, 126 (2007)
- "The effect of yttrium dopant on the proton conduction pathways of $BaZrO_3$, a cubic perovskite" Maria A. Gomez, Mythili Chunduru, Lorencia Chigweshe, Leigh Foster, S. J. Fensin, Katharyn M. Fletcher, and Laura E. Fernandez *Journal of Chemical Physics*, 132 (2010)
- "Structural heterogeneity in transmembrane Amyloid Precursor Protein homodimer is a consequence of environmental selection" Laura Dominguez,

Leigh Foster, Stephen C. Meredith, John E. Straub, and Dave Thirumalai *(Journal of the American Chemical Society)*, 136 (2014)

- "Engineered mutations to residue K28 affect the structure and positioning of APP-C99 peptide in lipid bilayer" Leigh Foster and John E. Straub *(in preparation)*

- "Transmembrane domain homodimer of Amyloid Precursor Protein adopts multiple conformational substates in lipid bilayers" Leigh Foster, Laura Dominguez, Stephen C. Meredith, John E. Straub, and David Thirumalai *(in preparation)*

- "Impact of membrane lipid composition on the structure and stability of homodimers of the transmembrane domain of Amyloid Precursor Protein" Laura Dominguez, Leigh Foster, John E. Straub, and David Thirumalai *(in preparation)*

- "Flemish A21G familial Alzheimer's Disease mutation alters APP-C99 homodimer interface" Leigh Foster and John E. Straub *(in preparation)*